Apatites Record Sedimentary Provenance Change 4–5 Myrs Before Clay in the Oligocene/Miocene Alpine Molasse

Julian Hülscher[1]*, Edward R. Sobel[2], Niklas Kallnik[1], J. Elis Hoffmann[1], Ian L. Millar[3], Kai Hartmann[1] and Anne Bernhardt[1]

[1]Institute of Geological Sciences, Freie Universität Berlin, Berlin, Germany, [2]Institut für Geowissenschaften, Universität Potsdam, Potsdam, Germany, [3]Geochronology and Tracers Facility, British Geological Survey, Keyworth, United Kingdom

Extracting information about past tectonic or climatic environmental changes from sedimentary records is a key objective of provenance research. Interpreting the imprint of such changes remains challenging as signals might be altered in the sediment-routing system. We investigate the sedimentary provenance of the Oligocene/Miocene Upper Austrian Northern Alpine Foreland Basin and its response to the tectonically driven exhumation of the Tauern Window metamorphic dome (28 ± 1 Ma) in the Eastern European Alps by using the unprecedented combination of Nd isotopic composition of bulk-rock clay-sized samples and partly previously published multi-proxy (Nd isotopic composition, trace-element geochemistry, U-Pb dating) sand-sized apatite single-grain analysis. The basin offers an excellent opportunity to investigate environmental signal propagation into the sedimentary record because comprehensive stratigraphic and seismic datasets can be combined with present research results. The bulk-rock clay-sized fraction εNd values of well-cutting samples from one well on the northern basin slope remained stable at ~−9.7 from 27 to 19 Ma but increased after 19 Ma to ~−9.1. In contrast, apatite single-grain distributions, which were extracted from 22 drill-core samples, changed significantly around 23.3 Ma from apatites dominantly from low-grade (<upper amphibolite-facies) metamorphic sources with Permo-Mesozoic and late Variscan U-Pb ages and εNd values of −4.4 to dominantly high-grade metamorphic apatites with late Variscan U-Pb ages and εNd values of −2.2. The change in apatite single-grain distributions at 23.3 Ma is interpreted to result from the exposure of a new Upper Austroalpine source nappe with less negative εNd values triggered by the ongoing Tauern Window exhumation. Combining these data with the clay-sized bulk-rock εNd values reveals that the provenance changed 4–5 Myrs later at 19 Ma in the clay-sized fraction. Reasons for the delayed provenance-change recording are rooted in the characteristics of the applied methods. Whereas single-grain distributions of orogen-wide sediment-routing systems can be dominated by geographically small areas with high erosion and mineral fertility rates, bulk-rock methods integrate over the entire drainage basin, thus diminishing extreme values. Hence, by combining these two methods, spatial

information are uncovered, enabling a previously unattained understanding of the underlying environmental change.

Keywords: apatite geochemistry and U-Pb dating, Nd isotopic composition, clay provenance, Northern Alpine Foreland Basin, Eastern Alps, Tauern Window, sediment routing system

INTRODUCTION

The infill of orogenic basins provides the primary source of information about an orogen's tectonic and climatic history. Changes in sediment flux, architecture, and/or provenance, so-called "environmental signals" (Romans et al., 2016; Tofelde et al., 2021), in these basins have been interpreted to reveal tectonic and climatic changes in the hinterland (Füchtbauer, 1964; Clift et al., 2008; Schlunegger and Castelltort, 2016; Tatzel et al., 2017; Blum et al., 2018; Huber et al., 2018). However, differentiating between a tectonically or climatically induced environmental signal exclusively by the induced change in the foreland remains challenging (Sharman et al., 2019; Zhang et al., 2020). Additionally, several processes in the sediment-transfer zone can interfere with signal transmission from source to sink, further hampering a correct interpretation (Murray et al., 2009; Jerolmack and Paola, 2010; Clift and Giosan, 2014; Schlunegger and Castelltort, 2016). This study addresses both problems by investigating signal propagation of the well-studied tectonically induced exhumation of the Tauern Window metamorphic dome in the European Eastern Alps, determining if and how this signal is expressed by changing provenance in its adjacent foreland. We use the unprecedented combination of bulk-rock clay-sized sediment Nd isotope and single-grain Sm-Nd isotope analyses on sand-sized apatites. The apatite single-grain distribution is complemented by available apatite trace-element geochemistry, fission track, and U-Pb age data on the same grains (Hülscher et al., 2021). Two main research questions are examined in this context: 1) Is there a delay in provenance-change recording between different grain-

size fractions, as hypothesized by Tofelde et al. (2021)? 2) What insights can be gained by this delayed environmental signal recording about processes in the sediment-routing system (SRS) and/or the environmental perturbation?

The eastern Northern Alpine Foreland Basin (NAFB, **Figure 1**) in Upper Austria offers an excellent opportunity to investigate environmental signal propagation as the evolution of the hinterland, the foreland and the SRS are relatively well constrained. We focus on the response of the sedimentary provenance to the tectonic exhumation of the Tauern Window metamorphic dome in the Eastern Alps from 28 ± 1 Ma onward; this event caused uplift and cooling in the overlying Upper Austroalpine nappes (Favaro et al., 2015; Reddy et al., 1993; Schneider et al., 2015). The propagation of this tectonic signal through the paleo-Inn SRS into the Upper Austrian NAFB (**Figure 2**) is well constrained by thermochronological results from sand and gravel deposits (Brügel et al., 2003; Kuhlemann et al., 2006; Dunkl et al., 2009; Hülscher et al., 2021). The evolution of the Upper Austrian NAFB has been constrained by extensive sedimentological studies on a large-scale ($>6,400 km^2$, >5 km depth) 3D seismic-reflection dataset provided by RAG Austria AG (Vienna) (De Ruig and Hubbard, 2006; Hinsch, 2008; Covault et al., 2009; Hubbard et al., 2009; Bernhardt et al., 2012; Masalimova et al., 2015; Kremer et al., 2018) as well as by stratigraphic studies (Grunert et al., 2013; Grunert et al., 2015; Hülscher et al., 2019) and provenance analysis on zircons (Sharman et al., 2018) and apatites (Hülscher et al., 2021).

We focus on the Chattian to Burdigalian infill of the basin (**Figure 3**), from which we sampled drill cores (for apatite
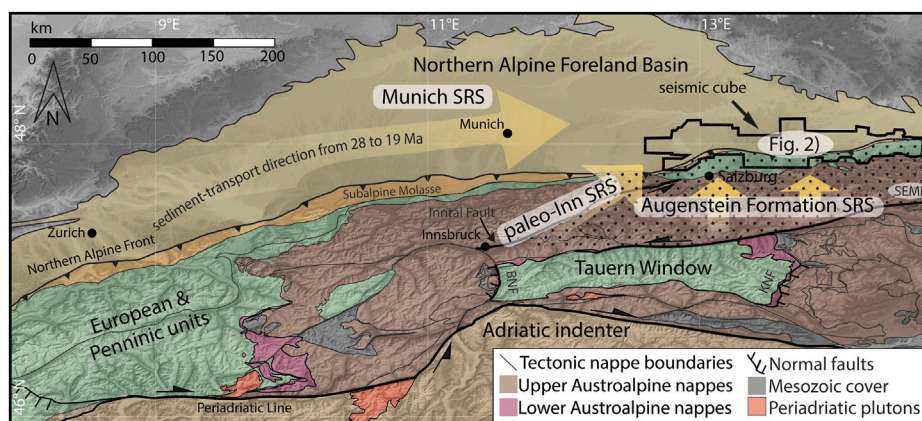
FIGURE 1 | Simplified geological map of the Alps showing the Tauern Window in the east bounded by two normal faults [after Schmid et al. (2004)]. The location of the seismic reflection cube in the Upper Austrian NAFB is enlarged in **Figure 2**. The three different sediment-routing systems (SRS) to the Upper Austrian NAFB are indicated by yellow arrows. SEMP = Salzach-Ennstal-Mariazell-Puchberg Fault; BNF = Brenner Normal Fault, KNF = Katschberg Normal Fault.
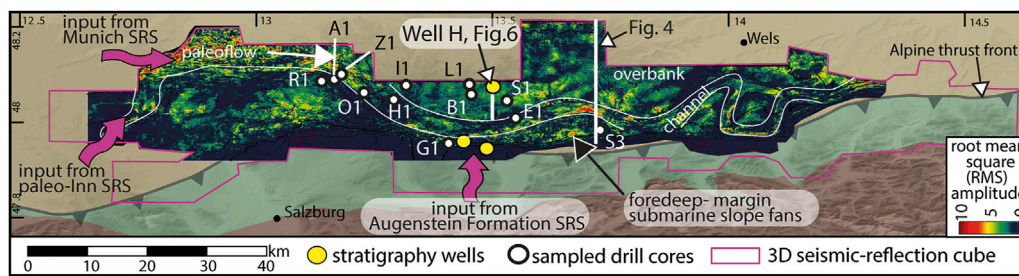
FIGURE 2 | Simplified geological map of the eastern NAFB in Upper Austria showing the locations of the sampled drill cores, Well H, and the wells with the stratigraphic information in the study area (Hülscher et al., 2019). The inset shows an RMS amplitude map in the Hall Formation outlining the meandering axial channel, the extensive northern overbank deposits, and the slope fans on the southern, tectonically active margin.

analysis) and well-cuttings (for clay analysis). The calculation of total signal-lag times [*sensu* Tofelde et al. (2021)] for the analyzed grain-size fractions indicate that the sand-sized single-grain apatites record the provenance change 4–5 Myrs earlier than the bulk-rock clay-sized sediment fraction. We suggest that this delay is controlled by the characteristics of the methods applied, as the single-grain distribution is dominated by the geographically small area with high erosion rates above the future Tauern Window. Bulk-rock methods integrate over the entire drainage area, diminishing extreme values and causing the provenance change to remain unrecorded in the sedimentary record until 19.0 Ma, when the SRS experienced a significant rearrangement, and the study area transitioned from the marine transfer zone to the final marine sink.

ND ISOTOPIC COMPOSITION AS PROVENANCE TOOL IN CLAYS AND APATITES

In this study we combine single-grain analysis of detrital sand-sized apatites and bulk-rock clay-sized sediments. Bulk-rock Nd isotope analysis has been used as a provenance tool for four decades as Nd isotope ratios are assumed to be relatively unaffected by transport and diagenetic processes (McCulloch and Wasserburg, 1978; Goldstein and Jacobsen, 1988; Goldstein and Hemming, 2003; Garçon et al., 2013) as well as variations in grain size (Goldstein et al., 1984; Garçon et al., 2013; Jonell et al., 2018). Even if different grain-size fractions have different absolute εNd values, the εNd values follow the same trend when sediment provenance changes (Jonell et al., 2018).
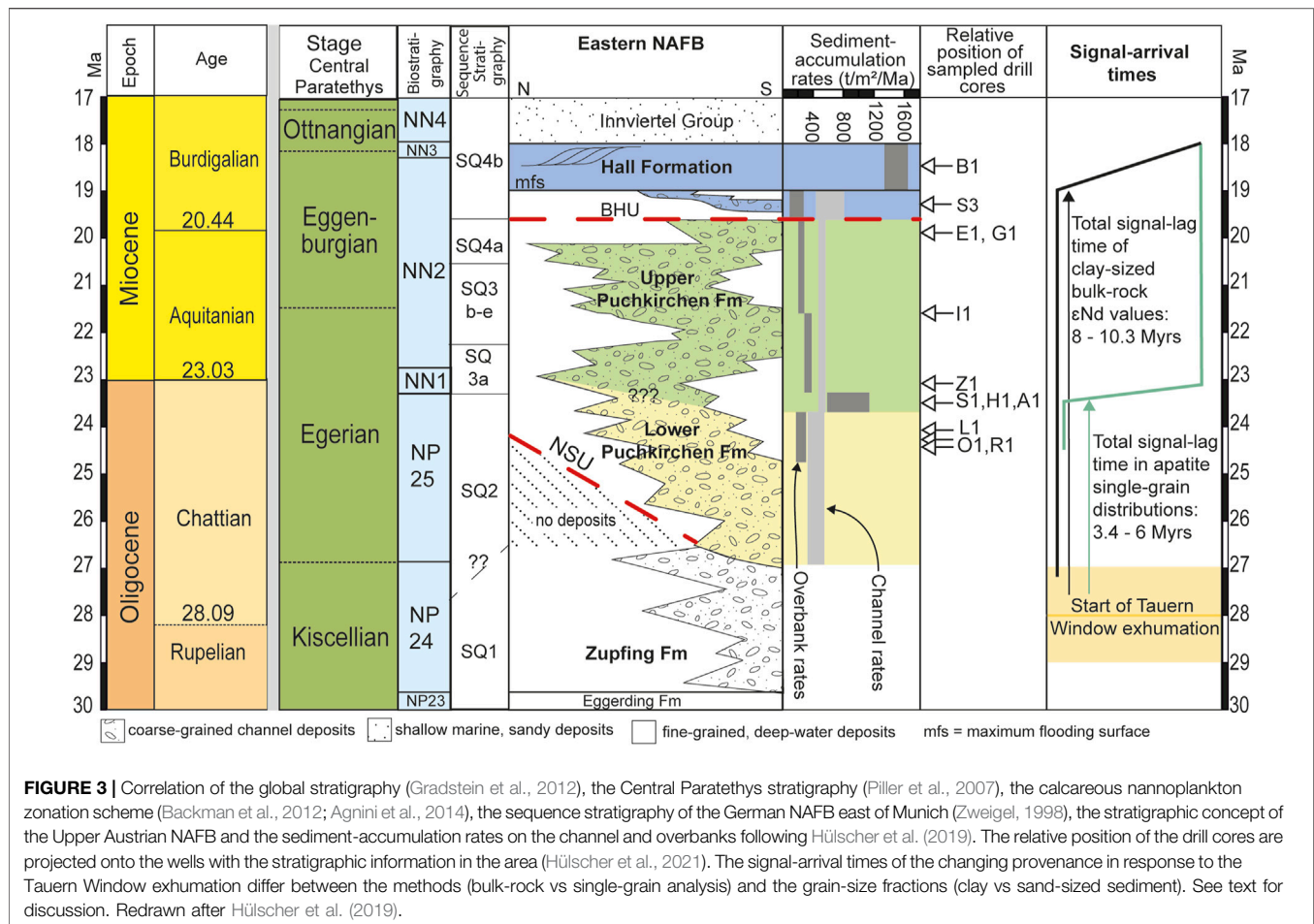
Geochemical (Dill, 1994; Morton and Yaxley, 2007; O'Sullivan et al., 2020) and fission-track analysis (Gleadow and Lovering, 1974; Garver et al., 1999; Frisch et al., 2001) of apatites have long been used to gain sedimentary provenance information. The developments of high throughput LA-Q-ICP-MS analyses and age reference correction procedures (Chew et al., 2014) have led to an increasing number of studies investigating apatite U-Pb isotopic and trace-element composition in the last decade (Henrichs et al., 2018; Mark et al., 2016; O'Sullivan et al., 2018). Recently, O'Sullivan et al. (2020) developed an apatite-discrimination scheme based on a LREE vs Sr/Y biplot, which allows a separation of the detrital apatites into six source-rock

types (alkali-rich igneous rocks [ALK]; mafic I-type granitoids and mafic igneous rocks [IM]; low-and medium-grade metamorphic [<upper amphibolite-facies] and metasomatic rocks [LM]; partial-melts/leucosomes/high-grade metamorphic rocks [HM]; S-type granitoids and high aluminum saturation index [>1.1] "felsic" I-types [S]; ultramafic rocks including carbonatites, lherzolites and pyroxenites [UM]). *In-situ* apatite Sm-Nd isotope analysis is another useful provenance tool as apatites record the Sm-Nd isotopic composition of their host rock during the pressure-temperature-time path of a magmatic or metamorphic event (Foster and Vance, 2006). Apatites of any given age lie on a $^{143}Nd/^{144}Nd$ vs. $^{147}Sm/^{144}Nd$ isochron (Hoinkes et al., 1997) and in young apatites (<60 Ma) the α-decay of ^{147}Sm to ^{143}Nd is too slow ($t_{1/2}$ = 106 Ga) to significantly change their $^{143}Nd/^{144}Nd$ values (Foster and Carter, 2007). However, in grains >100 Ma the radioactive decay of ^{147}Sm changes the $^{143}Nd/^{144}Nd$ value significantly. A comparison of εNd values of host rock and apatite is hampered by the Sm enrichment of apatite compared to the whole rock (Belousova et al., 2002; Henrichs et al., 2018). Furthermore, the depletion of REE in LM apatites (O'Sullivan et al., 2020) hampers the Sm-Nd isotope analysis of these grains, posing an unavoidable bias of the results.

GEOLOGICAL OVERVIEW
Evolution of the Cenozoic Northern Alpine Foreland Basin

The NAFB extends for ~1,000 km from Switzerland to Austria (**Figure 1**). Its Cenozoic evolution is connected to the approaching Adriatic plate, which is responsible for the loading and flexural bending of the distal southern European continental margin (Sinclair, 1997; Kuhlemann and Kempf, 2002). From 28 Ma onward, continental Molasse-type sedimentation dominated the Swiss and German parts of the basin (Kuhlemann and Kempf, 2002). These sediments were shed northward from the evolving Alps and were redirected eastward in the basin to a delta east of Munich (Füchtbauer, 1964). In contrast, the NAFB east of Munich remained deep marine (Rögl et al., 1979) from ~28 to 18.3 Ma (Grunert et al., 2013), notwithstanding, an eastward sediment routing also prevailed there (De Ruig and Hubbard, 2006).

FIGURE 3 | Correlation of the global stratigraphy (Gradstein et al., 2012), the Central Parathethys stratigraphy (Piller et al., 2007), the calcareous nannoplankton zonation scheme (Backman et al., 2012; Agnini et al., 2014), the sequence stratigraphy of the German NAFB east of Munich (Zweigel, 1998), the stratigraphic concept of the Upper Austrian NAFB and the sediment-accumulation rates on the channel and overbanks following Hülscher et al. (2019). The relative position of the drill cores are projected onto the wells with the stratigraphic information in the area (Hülscher et al., 2021). The signal-arrival times of the changing provenance in response to the Tauern Window exhumation differ between the methods (bulk-rock vs single-grain analysis) and the grain-size fractions (clay vs sand-sized sediment). See text for discussion. Redrawn after Hülscher et al. (2019).
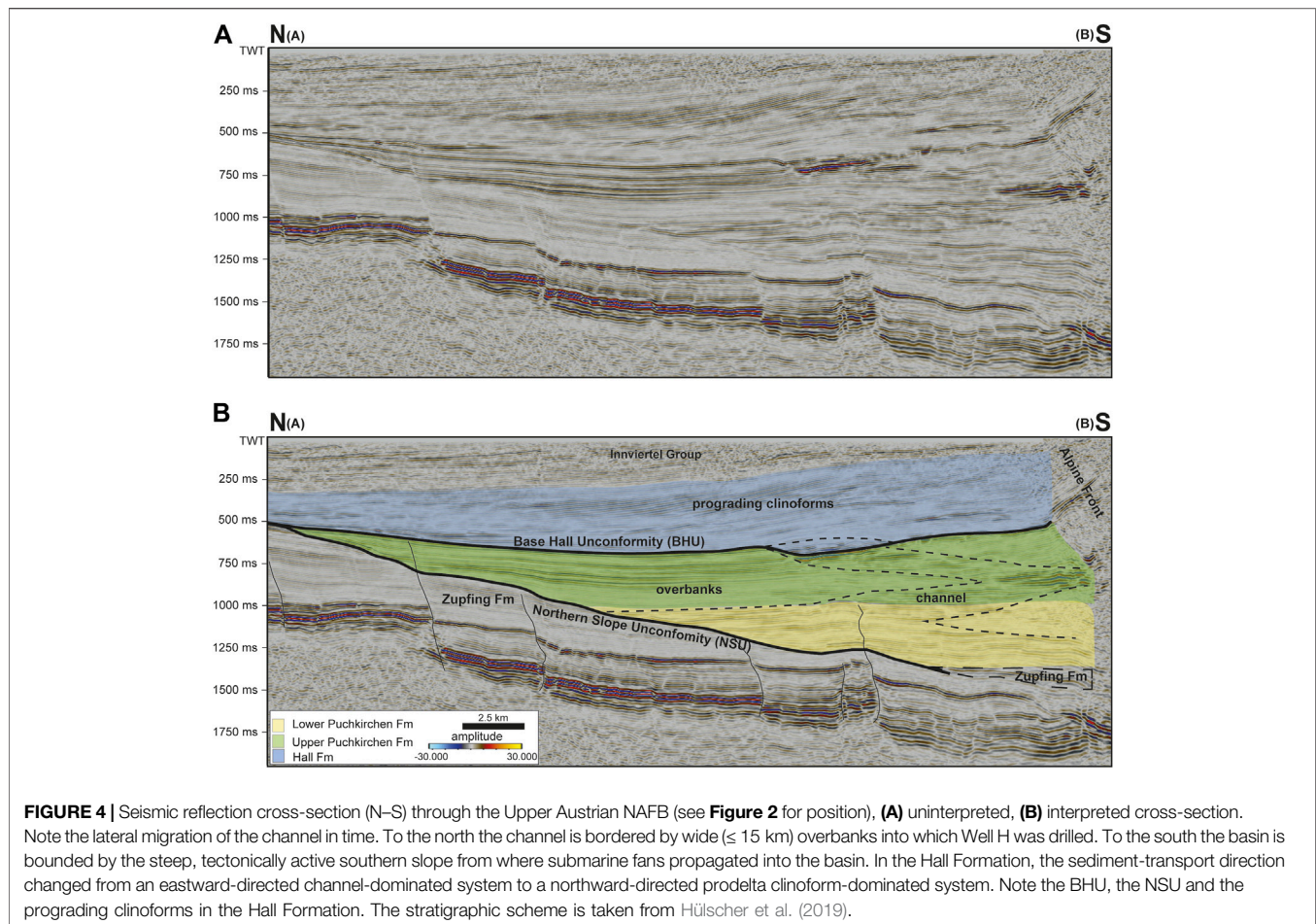
In the Upper Austrian part of the basin, depositional processes were controlled from ~28 Ma onward by a 3–6 km wide, deep-marine, gravity-flow dominated channel system that transported sediment eastward for >100 km (**Figures 2**, **4**). Submarine channel sedimentation lasted for more than 8 Myrs (Hülscher et al., 2019). The Zupfing Formation (ZFM), the Puchkirchen Group (Lower (LPF) and Upper Puchkirchen Formation (UPF)) and the basal Hall Formation (**Figure 3**) are characterized by structured and structureless sandstones, clast- and matrix-supported conglomerates and silty marls along the basin axis (Bernhardt et al., 2012; De Ruig and Hubbard, 2006; Hubbard et al., 2009). These channelized deposits of sediment-density flows (mostly turbidity currents and debris flows) are bounded towards the north (**Figure 4**) by wide (≤15 km) overbanks where sedimentation was controlled by hemipelagic settling and northward-directed overspill of sediment by density flows in the channel, resulting in a dominance of silty marls and less abundant turbiditic sandstones (Hubbard et al., 2009; Masalimova et al., 2015). From the tectonically active southern basin margin (**Figure 4**), submarine fans prograde into the basin (Covault et al., 2009; Hinsch, 2008). Eastward channelized sediment transport ended in the Hall Formation (HFM, **Figures 3**, **4**) during a sea-level highstand at 19.0 Ma and dominantly northward sediment routing was established in the

entire NAFB (Hinsch, 2008; Grunert et al., 2013; Garefalakis and Schlunegger, 2019; Hülscher et al., 2019). The Upper Austrian NAFB shallowed from deep-marine conditions to water depth <200 m within the next 0.7 Myrs (Grunert et al., 2013).

The Northern Slope Unconformity (NSU) and the Base Hall Unconformity (BHU, **Figure 3**) form two major basin-wide unconformities (De Ruig and Hubbard, 2006; Masalimova et al., 2015). Whereas an oversteepening of the northern slope caused the NSU during the initial deepening of the basin between 28.1 and 26.9 Ma (Masalimova et al., 2015; Hülscher et al., 2019), the BHU (~19.6 Ma) represents a non-depositional period on the overbanks and probably in the channel (Hülscher et al., 2019).

Tauern Window Exhumation as External Perturbation and Alpine Sediment-Routing Systems in the Oligocene/Miocene

The external perturbation that we interpret to have caused the environmental signal in the studied succession is related to the beginning exhumation of the greenschist-to amphibolite-facies metamorphic rocks (Schmid et al., 2013) nowadays exposed in the Tauern Window metamorphic dome (**Figure 1**) (Hülscher et al., 2021), hereafter referred to as Tauern Window exhumation. This exhumation was triggered by the Adriatic indentation into

FIGURE 4 | Seismic reflection cross-section (N–S) through the Upper Austrian NAFB (see **Figure 2** for position), **(A)** uninterpreted, **(B)** interpreted cross-section. Note the lateral migration of the channel in time. To the north the channel is bordered by wide (≤ 15 km) overbanks into which Well H was drilled. To the south the basin is bounded by the steep, tectonically active southern slope from where submarine fans propagated into the basin. In the Hall Formation, the sediment-transport direction changed from an eastward-directed channel-dominated system to a northward-directed prodelta clinoform-dominated system. Note the BHU, the NSU and the prograding clinoforms in the Hall Formation. The stratigraphic scheme is taken from Hülscher et al. (2019).

the Eastern Alps (Favaro et al., 2015). After the end of the Barrovian-type metamorphism in the subducted and thickened European crust between 40 and 30 Ma, the ongoing convergence between the upper Adriatic and the lower European plate led to large-scale upright folding of the Penninic units of the future Tauern Window (Cliff et al., 1985; Favaro et al., 2015; Scharf et al., 2013; Schneider et al., 2015). This folding caused uplift and cooling (~28 Ma, Rb-Sr in white mica) in the Penninic units (Reddy et al., 1993; Favaro et al., 2015) and exhumation and denudation in the overlying Upper Austroalpine nappes, which caused a provenance change in the nearby foreland (Hülscher et al., 2021). Apatite single-grain analysis on northern slope and channel samples of the Puchkirchen Group and HFM samples revealed a change in the trace-element geochemistry and U-Pb data around 23.3 Ma (Hülscher et al., 2021). LREE-enriched apatites with >1,000 ppm (LPF: 6%, HFM: 23%) and Sr/Y values < 0.1 (LPF: 24%, HFM: 38%) increased at 23.3 Ma and reached a maximum in the HFM (**Figure 5**). Contemporaneously, the number of apatites yielding late Variscan U-Pb ages increased. Based on the discrimination diagram of O'Sullivan et al. (2020), Hülscher et al. (2021) interpreted the change in apatite trace-element geochemistry to mirror a change in source rocks from a dominance of low-grade metamorphic sources before 23.3 Ma to high-grade

metamorphic sources thereafter. Combined with the increasing number of late Variscan U-Pb ages, this indicates an increasing input from a high-grade, late Variscan metamorphic source (**Figure 5**) from 23.3 Ma onward driven by the early exhumation of the Tauern Window (Hülscher et al., 2021). In this period of early (28 ± 1 Ma) and slow (0.3–0.6 mm/a) exhumation (Hülscher et al., 2021), orogen-perpendicular shortening caused the surface response (Favaro et al., 2017). A reorganization to orogen-parallel extension *via* low-angle normal faults at the eastern and western end of the Tauern Window around 23–21 Ma (**Figure 1**) (Favaro et al., 2015; Favaro et al., 2017) resulted in a doubling of exhumation rates (1.5–2 mm/a) in the future Tauern Window area (Frisch et al., 2000). The Penninic units in the Tauern Window reached the surface around 13 Ma when Penninic pebbles appeared in the Upper Austrian NAFB (Brügel et al., 2003).

Three SRSs have been suggested to contribute sediment to the Upper Austrian NAFB. 1) The majority of the Eastern Alps drained northeastward from Oligocene onward *via* the paleo-Inn (**Figure 1**) (Brügel et al., 2003; Hülscher et al., 2021; Sharman et al., 2018). The river flowed through the Inn valley and built up alluvial and marine deposits of the Inntal-Tertiary in the Inn valley and the Chiemgau, Wachtberg and Munderfinder-Kobernhauser-Hausruck Fan

FIGURE 5 | Sand-sized apatite single-grain analyses. **(A)** Kernel density estimation plot of the U-Pb ages of the detrital apatites separated based on their trace-element geochemistry and the discrimination diagram of O'Sullivan et al. (2020). All apatite groups show a strong late Variscan/early Permian (250–350 Ma) peak. The IM and LM grains also show Mesozoic, Eoalpine and Alpine ages. **(B)** Distribution of the apatite εNd values of the individual apatite groups. Vertical bars represent the median of the distributions. Note the significantly higher εNd values in the HM apatites. **(C)** Evolution of apatite characterization plotted against the depositional ages. The share of HM apatites increase from ~20% to ~40% at 23.3 Ma. Apatite samples between 19.6 and 19.0 Ma are excluded from the trend because fission track and foraminiferal analysis indicate that these samples contain recycled sediment (Grunert et al., 2013; Hülscher et al., 2021). Uncertainties are based on the uncertainties of the depositional ages and the probability of possible apatite misclassification based on the discrimination success rate (O'Sullivan et al., 2020). *n* = number of analyzed apatites. Data of **(A)** and **(C)** from Hülscher et al. (2021), data of **(B)** is presented in this study. The apatites from S-type granitoids and HM sources, as differentiated by O'Sullivan et al. (2020), are grouped as HM apatites for simplicity.

deposits (**Figure 1**) in the Upper Austrian NAFB (Brügel et al., 2003; Ortner and Stingl, 2001). A direct connection from the Chiemgau Fan to the Puchkirchen channel system existed (De Ruig and Hubbard, 2006) (**Figures 1**, **2**). The southern drainage divide was located along to the Periadriatic Line (Brügel et al., 2000; Brügel et al., 2003) (**Figure 1**). The western boundary was located in the western Lower Austroalpine nappes in Miocene times (**Figure 1**) (Skeries and Troll, 1991). The detritus from this SRS was deposited on the southern and northern slope of the Puchkirchen channel system (Hülscher et al., 2021; Sharman et al., 2018). 2) Eastern Alpine material also entered the southern slope of the Upper Austrian NAFB *via* a southern SRS through the Augenstein Formation (**Figure 1**) (Frisch et al., 2001; Hülscher et al., 2021; Sharman et al., 2018). The Augenstein Formation accumulated on top of today's Northern Calcareous Alps, east of the Inn valley from 35–30 Ma onward, mainly sourced from the Austroalpine basement and its Mesozoic cover in the south (Frisch et al., 2001). Around 21 Ma, the initiation of exhumation of the Northern Calcareous Alps caused the erosion and redeposition of the Augenstein Formation into the Upper Austrian NAFB (Frisch et al., 2001; Hülscher et al., 2021). 3) A western SRS supplied material *via* a large delta system located close to Munich (hereafter Munich SRS) to the Puchkirchen channel system (**Figure 1**) in Oligocene/early Miocene times (Zweigel, 1998; Sharman et al., 2018). Central Alpine material was transported to the delta (Füchtbauer, 1964) in a meandering river system (Platt and Keller, 1992). The importance of this SRS for sand-sized sediment supply to the Puchkirchen channel system is debated (Sharman et al., 2018; Hülscher et al., 2021). With the reorganization of the SRS during the sea-level highstand around 19 Ma, the Munich SRS

was cut off from the Upper Austrian NAFB (Füchtbauer, 1967).

SAMPLES AND METHODS

Drill-cutting samples from Well H on the northern slope (**Figure 2**, **6**) were analyzed for the Nd isotopic composition of the clay-sized fraction. Each sample represents a mixture of 2 m sediment thickness. For Well H, a precise chemo- and biostratigraphic context was published previously (**Figure 3**, **6**) that constrained the depositional ages of the sediment (Hülscher et al., 2019). We consider sample contamination of the drill-cutting samples during the drill process by sediment movement and upward transport to play a subordinate role. The order of first occurrences of index fossils and the $\delta^{13}C_{carb}$ stratigraphy in these drill-cutting samples are in agreement with global records (Hülscher et al., 2019). Samples were taken in an interval from 2,380 to 900 m (measured depth from the surface). The ZFM, Puchkirchen Group and basal HFM samples (2,380–1,475 m) represent mostly deep-water hemipelagic overbank sedimentation (silty marlstones, **Figure 6**); however, some sand-rich layers have been sampled which probably represent turbiditic sandstones (Hubbard et al., 2009). Samples from the upper HFM (1,420–900 m) are again hemipelagic silty marlstones (**Figure 6**); however, their depositional environment had changed to a northward-prograding prodelta wedge (Hinsch, 2008).

The single-grain analyses were run on the same drill-core samples used by Hülscher et al. (2021) and the same sample-naming scheme was adopted in the present research. These authors sampled turbiditic sandstone in drill cores from the northern, central, and southern part of the basin. Each drill core was correlated within the 3D seismic-reflection dataset onto at least one of the wells with
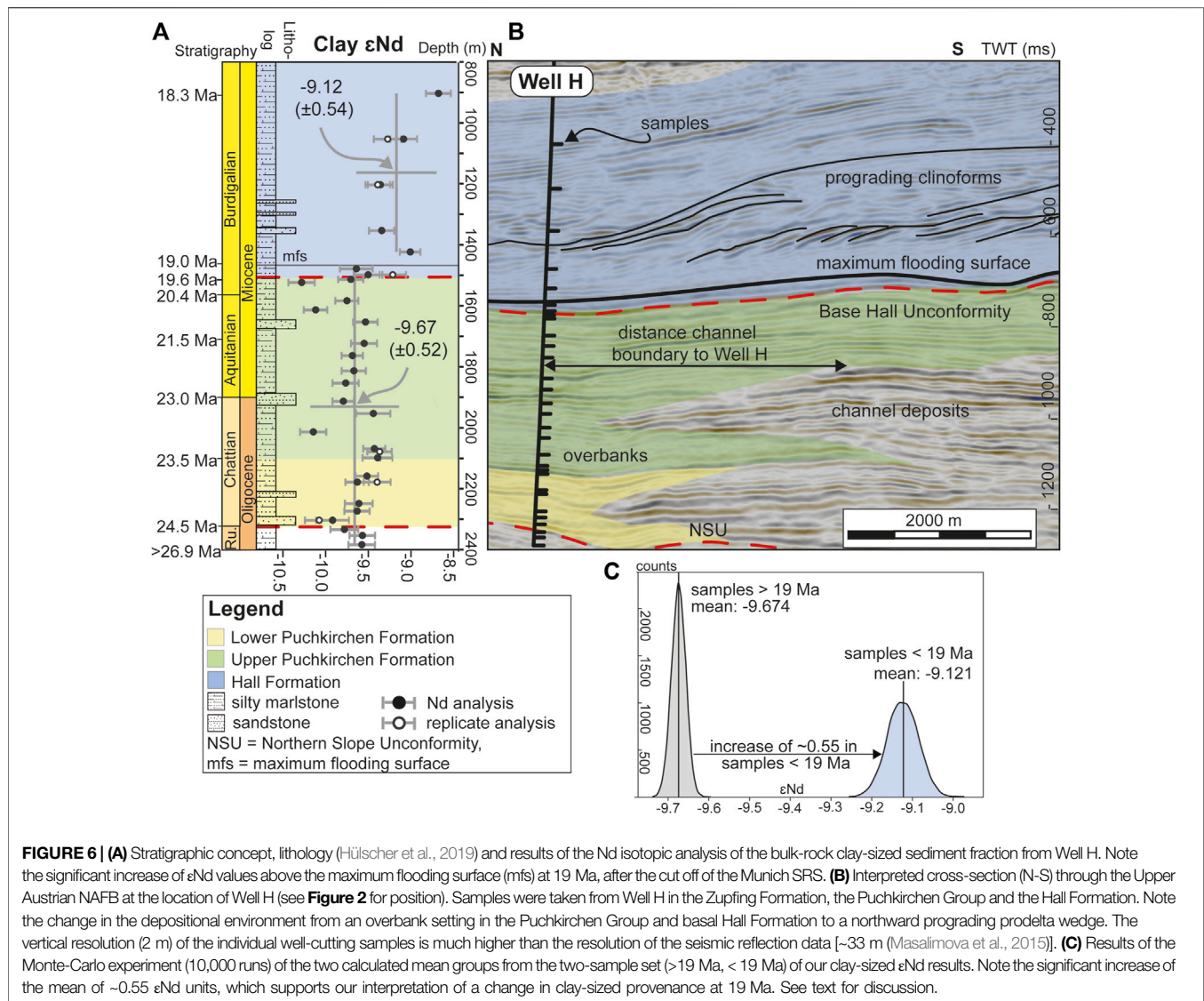
FIGURE 6 | (A) Stratigraphic concept, lithology (Hülscher et al., 2019) and results of the Nd isotopic analysis of the bulk-rock clay-sized sediment fraction from Well H. Note the significant increase of εNd values above the maximum flooding surface (mfs) at 19 Ma, after the cut off of the Munich SRS. **(B)** Interpreted cross-section (N-S) through the Upper Austrian NAFB at the location of Well H (see **Figure 2** for position). Samples were taken from Well H in the Zupfing Formation, the Puchkirchen Group and the Hall Formation. Note the change in the depositional environment from an overbank setting in the Puchkirchen Group and basal Hall Formation to a northward prograding prodelta wedge. The vertical resolution (2 m) of the individual well-cutting samples is much higher than the resolution of the seismic reflection data [~33 m (Masalimova et al., 2015)]. **(C)** Results of the Monte-Carlo experiment (10,000 runs) of the two calculated mean groups from the two-sample set (>19 Ma, < 19 Ma) of our clay-sized εNd results. Note the significant increase of the mean of ~0.55 εNd units, which supports our interpretation of a change in clay-sized provenance at 19 Ma. See text for discussion.

stratigraphic information (**Figure 2**) to constrain the depositional ages (Hülscher et al., 2021). For details about sample preparation, see Hülscher et al. (2021). We focused our campaign on samples from the northern slope and the channel of the Puchkirchen Group. However, samples G1 and S3 were taken from the southern slope (**Figure 2**). The apatites were previously irradiated for fission-track dating, covered with a thin film (<10 μm) of super glue and analyzed for their trace-element geochemistry and U-Pb ages with a Teledyne Photon Machines Analyte Excite 193 nm ArF Excimer laser-ablation system coupled to a Thermo Scientific iCAP-Q ICP-MS (Hülscher et al., 2021).

Nd Isotope Analyses in Clay-Sized Fraction by ICP-MS

The clay-size fraction from thirty well-cutting samples were analyzed for their Nd isotopic composition. This fraction was

separated by mixing the samples with distilled water and centrifuging them for 1 min at 4,000 rpm. The suspended fraction was decanted and dried. The separated clay-sized fractions were treated with 10% acetic acid and washed with Milli-Q water. Because all samples contained significant amounts of organic material, 30 samples were heated up to 830°C in a muffle furnace for combustion of organic materials. Additionally, six samples were selected for replicate analysis (**Figure 6**). In these cases, the organic material was removed by chemical treatment during digestion using HNO_3 and H_2O_2.

100 mg of sample material was digested in a 3:2 mixture of concentrated $HF-HNO_3$ at 120°C for 24 h. After dry down, samples were treated three times with 2 ml HNO_3 and dried. This was followed by 12 h calibration in 6 M HCl. After dry down, each sample was taken up in calibrated 2.5 M HCl and centrifuged. The separation of Nd followed the protocol of Richard et al. (1976). The REE were separated using cation

exchange resin (AG 50WX8 resin) with HCl. After dry down at 120°C, the REE cuts were taken up in 0.15 M HCl and Nd was separated from other REE on columns using coated Teflon powder cation exchange resin (PTFE in HDEHP). After extraction, Nd cuts were dried at 120°C and dissolved in 1 ml 0.25 M HNO_3. Procedural blanks were <20 pg for the samples where organic matter was combusted. For the unheated samples, the procedural blank was <130 pg. All blanks were negligible, and no correction was necessary.

Samples were analyzed for their $^{143}Nd/^{144}Nd$ ratios with a Thermo Scientific Neptune Plus multi-collector inductively coupled plasma mass spectrometer at the Institut für Mineralogie (Westfälische Wilhelms-Universität Münster, Germany). JNdi-1 solution was used as reference material during analysis, revealing $^{143}Nd/^{144}Nd$ = 0.512096 (± 8, 2σ standard deviation, n = 17). The data is reported relative to JNdi-1 ($^{143}Nd/^{144}Nd$ = 0.512099 (Garçon et al., 2018)). Results were normalized to $^{146}Nd/^{144}Nd$ = 0.7219 using the exponential law and reported in εNd notation (DePaolo and Wasserburg, 1976) with 2σ uncertainties.

Nd and Sm Isotope Analyses in Sand-Sized Single-Grain Apatite by Laser Ablation MC-ICP-MS

Isotope analyses were carried out at the Geochronology and Tracers Facility, British Geological Survey, Keyworth, United Kingdom, using a Thermo Scientific Neptune Plus MC-ICP-MS coupled to a New Wave Research UP193UC Excimer laser ablation system. Helium was used as the carrier gas through the ablation cell with Ar make-up gas being connected *via* a T-piece and sourced from a Cetac Aridus II desolvating nebulizer. The instrument was tuned for low oxide production, and 0.008 l/min of nitrogen were introduced *via* the nebulizer in addition to Ar to minimize oxide formation.

For neodymium isotope analysis, $^{142}Ce+^{142}Nd$, ^{143}Nd, $^{144}Nd+^{144}Sm$, ^{145}Nd, ^{146}Nd, ^{147}Sm, ^{149}Sm, ^{150}Nd and ^{151}Eu were measured simultaneously during static 30 s ablation analyses. Because of the relatively small grain size of the apatites, a 35 μm laser spot was used for most samples. Where grain size allowed, a 50 μm spot was used. The laser fluence was 8–10 J/cm^2. Correction for ^{144}Sm on the ^{144}Nd peak was carried out using the method of Yang et al. (2014). Madagascar apatite was used as the primary reference material for laser-ablation analysis. The Durango apatite reference material was also analyzed thought the analytical session, along with the standard glasses JNd-i, JNd-i LREE, and NIST 610. Data reduction was carried out using the Iolite data reduction package (Paton et al., 2011). Analytical uncertainties for unknowns were propagated by quadratic addition to include the standard error of the mean of the analysis and the reproducibility of the Durango reference material. εNd values were calculated using a ^{147}Sm decay constant of 6.54×10^{-12} y^{-1} (DePaolo and Wasserburg, 1976), the present-day chondritic $^{147}Sm/^{144}Nd$ value of 0.1967, and $^{143}Nd/^{144}Nd$ ratio of 0.512638 (Jacobsen and Wasserburg, 1980).

RESULTS

Neodymium Isotopic Composition of the Clay-Sized Fraction

Results from 30 neodymium isotopic analyses of the clay-sized fraction samples are reported. Six replicates yield similar results within their 2σ error when compared to the original sample (**Figure 6**). The εNd values show little variation in the ZFM (three samples), the LPF (six samples) and the UPF (16 samples) around a mean of −9.73 (±0.52; **Figure 6**). In the lower part of the HFM, two samples (1,495 m, 1,475 m) reveal similar values when compared to samples from the UPF. Five samples above 1,420 m in the HFM show higher εNd values (mean: −9.12 ± 0.52; **Figure 6**) when compared to the earlier 25 samples.

We performed a Monte-Carlo experiment to test the robustness of this shift in εNd values. To provide a robust estimate of the shift in Nd isotope composition in mean and variance between the unbalanced subsamples for >19 Ma [n_1 = 25 (four replicate measurements)] and for <19 Ma [n_2 = 5 (+2)] εNd measurements, we performed n_{MC} = 10,000 random sampling from each measurement assuming a normally distributed measurement error (**Figure 6**; μ and 2σ-interval). Replicate measurements have been randomly selected once for all n_{MC} samples. Statistical analyses were performed in R Vers. 4.0.2 using the stats package (R Core Team, 2020). The distribution of the n_{MC} random sample means appears normally distributed for both samples as expected by the Central Limit Theorem, with a mean μ_1 = −9.674 (σ_1 = 0.018, >19 Ma) and μ_2 = −9.121 (σ_2 = 0.038, <19 Ma). Therefore, we applied a Student's t-test, suggesting an increase of the mean εNd value of the two subsample sets of 0.5520–0.5536 with 95%-confidence and p-value < 10^{-15} under the assumption of heteroscedasticity. Therefore, we regard the two subsample sets (>19 Ma, < 19 Ma) as being significantly different.

Apatite Single-Grain Results

The detrital apatite trace-element geochemistry and U-Pb data was taken from Hülscher et al. (2021). Based on the discrimination diagram of O'Sullivan et al. (2020), Hülscher et al. (2021) grouped the detrital apatites into four source rocks: mafic igneous rocks (IM); low- and medium-grade metamorphic (<upper amphibolite-facies) (LM); high-grade metamorphic rocks (HM); and ultramafic rocks (UM). The apatites from S-type granitoids and HM sources, as differentiated by O'Sullivan et al. (2020), were grouped with the HM apatites for simplicity.

The $^{147}Sm/^{144}Nd$ and $^{143}Nd/^{144}Nd$ ratios of 406 sand-sized detrital apatite grains further constrain the differences between the proposed apatite groups based on their trace-element geochemistry. εNd values range between −14.63 and 10.34 (median: −4.09) and are highest in the HM apatite group (median: −1.95) (**Figure 5**). LM, IM, and UM apatites have similar εNd single-grain distributions (**Table 1**; **Figure 5**). The $^{147}Sm/^{144}Nd$ ratios are similar between all different apatite groups (**Table 1**). A Kolgomorov–Smirnov (K-S) Test (Hodges, 1958) was performed to test whether the εNd single-grain distributions of the different apatites groups resulted from random sampling of the same parent population or was significantly different. p-values of the K-S Test of the HM apatites are <0.01% when compared to

TABLE 1 | Results of the apatite Sm-Nd analysis and their statistical analysis of the different subgroups.

Number of grains		LM	HM	UM	IM
		127	173	10	96
εNd	Median	−4.88	−1.95	−7.18	−5.85
	5th percentile	−10.46	−9.37	−11.24	−10.39
	95th percentile	2.57	3.00	1.03	0.64
^{147}Sm/^{144}Nd	Median	0.28100	0.27044	0.23302	0.26414
	5th percentile	0.21279	0.169758	0.132629	0.110525
	95th percentile	0.44667	0.413336	0.3311585	0.380225
KS-test *p*-values εNd distribution	LM	–	0%	27%	11%
	HM	–	–	0%	0%
	UM	–	–	–	56%

the remaining apatite groups, indicating a significantly different εNd distribution of the HM group, in contrast to the remaining apatite groups which show similar εNd distributions (**Table 1**).

Our dataset is biased towards apatites with high Sm and Nd contents and this bias especially influences the results from the LM apatites. Apatites from low-grade metamorphic sources are usually depleted in REE (Henrichs et al., 2018; O'Sullivan et al., 2020), making their Sm-Nd isotopic analysis difficult. LM apatites are underrepresented in our Nd isotope dataset (31%) compared to the trace-element dataset (47%) of Hülscher et al. (2021).

INTERPRETATION

Provenance Information From Clay-Sized Sediment and Apatites

The clay-sized bulk-rock εNd values remained stable around −9.67 (±0.52) from ~27 Ma to 19 Ma. In the five samples younger than 19 Ma, a significant increase of 0.55 εNd units to −9.12 (±0.54) (**Figure 6**) was found. No correlation between the data and the proximity of the channel or the lithology are recognizable (**Figure 6**). Gier (1998) reported a diagenetic clay mineral transformation from smectite to illite which linearly increases with depth. The described step-change at 19 Ma in the clay-sized bulk-rock εNd values cannot be explained by this linearly increasing clay transformation, as such a trend is not noticeable in the results. In parts of the basin (e.g., in the basal Hall Formation and in a gas field 10 km east of Well H in the lower part of the UPF, **Figure 2**) methanogenesis has been described as an important diagenetic process (Schulz et al., 2009; Grundtner et al., 2016). The εNd values do not show significant fluctuations in the basal Hall Formation or the lower part of the UPF of Well H (**Figure 6**). Hence, we interpret our clay-sized εNd values to be unaffected by the diagenetic processes in the basin.

Regional climatic reconstructions suggested a stable warm and humid climate during the Oligocene/Early Miocene (Mosbrugger et al., 2005; Grunert et al., 2014; Filek et al., 2021) with mean annual precipitation rates consistently >900 mm in the foreland (Mosbrugger et al., 2005). As climatic records are still sparse from the NAFB, we cannot exclude the possibility that climatic fluctuations on timescales below 1 Myrs have occurred. However, based on the available data, the bulk-rock clay-sized

εNd results do not appear to have been significantly affected by climatic changes and represent a reliable provenance proxy, governed by tectonic processes.

Potential source rocks for the clay-sized fraction in the ~27 to 19 Ma samples are located in the Eastern Alps, as suggested by provenance reconstructions of sand-sized sediment (Hülscher et al., 2021; Sharman et al., 2018). However, Upper Chattian and Aquitanian deposits from the Swiss NAFB show similar bulk rock εNd values of ~−9.7 (Henry et al., 1997). A connection of the Swiss NAFB to the Munich delta *via* a meandering river system
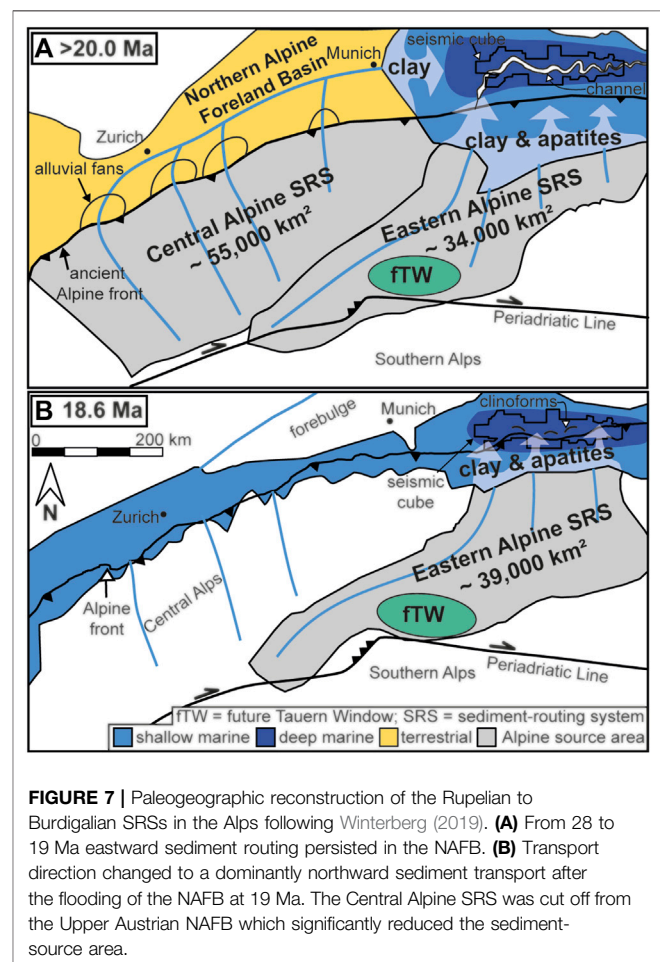

FIGURE 7 | Paleogeographic reconstruction of the Rupelian to Burdigalian SRSs in the Alps following Winterberg (2019). **(A)** From 28 to 19 Ma eastward sediment routing persisted in the NAFB. **(B)** Transport direction changed to a dominantly northward sediment transport after the flooding of the NAFB at 19 Ma. The Central Alpine SRS was cut off from the Upper Austrian NAFB which significantly reduced the sediment-source area.

(Platt and Keller, 1992), which was rich (70%–80%) in silt and clay, has been suggested based on heavy mineral assemblages (Füchtbauer, 1964; Füchtbauer, 1967). During the UPF and basal HFM, the delta was connected to the Puchkirchen channel system *via* the Halfinger Canyon (**Figure 2**) (Zweigel, 1998). This Munich SRS had a larger source area than the Eastern Alpine SRSs of the paleo-Inn and the Augenstein Formation (**Figure 7**) (Winterberg, 2019). We regard the Munich SRS to be a major contributor to the Upper Austrian NAFB clay-sized sediments >19 Ma due to the increasing εNd values after the tectonically induced (Zweigel, 1998) cut-off of the Munich SRS (Füchtbauer, 1967) at 19 Ma (**Figure 6**). However, the clay-sized sediment provenance before 19 Ma is likely to represent a mixture of Central and Eastern Alpine sources, as an Eastern Alpine source is reported for the sand-sized fraction (Sharman et al., 2018; Hülscher et al., 2021).

In the five <19 Ma clay-sized samples, εNd values increased to −9.12 ± 0.52. An explanation for this changing provenance might be related again to processes in the Swiss NAFB. Henry et al. (1997) reported bulk-rock εNd values of ~−8.2 from the Swiss NAFB from the beginning of the Burdigalian (~20.4 Ma); these might have caused the increase in clay-sized bulk-rock εNd values in the Upper Austrian NAFB. Based on detrital zircon U-Pb ages, Sharman et al. (2018) suggested that the Hall Formation may have received sediment from the Bohemian Massif, where granitoids with less negative εNd values (~−1 to −9) are reported (Finger et al., 1997; Liew and Hofmann, 1988; Teipel et al., 2004). However, both sources seem unlikely to be the driver for the clay-sized provenance change as the major sediment-transport direction became north-directed in the Upper Austrian NAFB (**Figure 4**, **6**) from 19 Ma onward (Hinsch, 2008; Grunert et al., 2013; Hülscher et al., 2019).

This tectonically-driven (Zweigel, 1998) switch in sediment-transport direction from eastward transport before 19 Ma (Platt and Keller, 1992; Füchtbauer, 1964; De Ruig and Hubbard, 2006) to northward transport thereafter in the entire NAFB (Hinsch, 2008; Garefalakis and Schlunegger, 2019; Hülscher et al., 2019) went along with evolution of the Upper Austrian NAFB from a marine transfer zone to a marine terminal sink (Hülscher et al., 2019). A four-fold increase in sediment-accumulation rates (**Figure 3**), submarine channel sedimentation cessation and prodelta-wedge northward-progradation reflect this evolution (De Ruig and Hubbard, 2006; Hinsch, 2008; Grunert et al., 2013; Hülscher et al., 2019). As the basin evolved from an Alpine-wide transfer zone to an Eastern-Alpine marine terminal sink (Hülscher et al., 2019), the clay-sized sediment provenance switched from a mixed Alpine-wide one to a local Eastern Alpine one, resulting in significantly less negative εNd values in the samples <19 Ma (**Figure 6**).

Potential source rocks for the clay-sized bulk-rock εNd values after <19 Ma are the Upper Austroalpine nappes in the Eastern Alps (**Figure 1**). As bulk-rock εNd values between −5 and −15 are quite common in all Eastern Alpine nappe systems (**Supplementary Figure S1**) (Thöni and Jagoutz, 1993; Bernhard et al., 1996; Thöni and Miller, 1996; Hoinkes et al., 1997; Thöni and Miller, 2000; Schuster et al., 2001; Thöni, 2003; Tumiati et al., 2003; Schulz et al., 2004; Thöni and Miller, 2004;

Habler et al., 2006; Thöni, 2006; Habler et al., 2007; Habler et al., 2009; Thöni and Miller, 2009; Thöni and Miller, 2010; Heinrichs et al., 2012), a source-rock interpretation just from the clay-sized bulk-rock εNd values is difficult, particularly since the values most likely represent a mixture of different Eastern Alpine sources. Provenance information from sand-sized apatites with comparable depositional ages suggests a high-grade metamorphic, late Variscan source with increased εNd values, potentially a part of the Ötztal-Bundschuh Nappe System (see discussion below). As apatites and clay-sized bulk-rock εNd values both evolve towards less negative εNd values, we interpret both to be governed by the erosion of parts of the Ötztal-Bundschuh Nappe System with increased εNd values, driven by the Tauern Window exhumation. However, from the clay-sized bulk-rock εNd values alone we cannot exclude other possible sources in the Eastern Alpine nappe stack.

Contrary to our interpretation of a stable clay-sized sediment provenance before 19 Ma, Hülscher et al. (2021) reported a change in sand-sized single-grain apatite provenance based on their trace-element geochemistry and U-Pb thermochronology dataset at 23.3 ± 0.3 Ma (**Figure 5**). These authors pointed out that the apatites were derived from the Eastern Alps because of the stable provenance after the cut-off of the Munich SRS at 19 Ma (**Figure 5**). This changing provenance at 23.3 Ma is assumed to be governed by the Tauern Window exhumation from 28 (±1) Ma onward (Hülscher et al., 2021). Contrary to that interpretation, Sharman et al. (2018) suggested an increasing sediment delivery from the Munich SRS (**Figure 1**) to explain the decreasing shares of zircon single-grain ages >525 Ma and increasing proportion of grain ages between 250 and 375 Ma from the LPF to UPF found by the authors.

Our new Sm-Nd isotopic dataset supports the idea that the change in apatite provenance at 23.3 (±0.3) Ma is related to processes in the Eastern Alps. The apatites are not only different in their trace-element geochemistry as shown by Hülscher et al. (2021) but also in their Nd isotope geochemistry (**Figure 5**) with the HM apatites having significantly less negative εNd values than the IM, LM, and UM grains (**Table 1**). Higher εNd values can be explained by two reasons: either the apatites differ significantly in their formation ages, or the $^{143}Nd/^{144}Nd$ ratio of the source rock is different (DePaolo and Wasserburg, 1976). Even though the combined U-Pb and Sm-Nd dataset does not contain both types of information for all grains, **Figure 5** shows that the U-Pb age distribution of all apatite subgroups are dominated by ages between 250 and 350 Ma. In combination with the slow ^{147}Sm decay ($6.54 \times 10^{-12}\,y^{-1}$) (DePaolo and Wasserburg, 1976), different formation ages seem to play a subordinate role in explaining the different εNd values between the apatite subgroups. Therefore, we interpret the difference to be inherited from the source rocks. The source rocks of the HM apatites must have had significantly higher εNd values compared to the IM, LM, and UM apatites source rocks (**Table 1**; **Figure 5**). This source became a significant contributor (~40% HM apatites) for the sand-sized sediment in the Upper Austrian NAFB after 23.3 Ma (**Figure 5**) (Hülscher et al., 2021). The Ötztal-Bundschuh nappe system contains gneisses which experienced an upper

amphibolite to eclogite facies metamorphic event in Variscan times (Hoinkes et al., 1997; Rode et al., 2012; Schulz et al., 2019) and have enriched $^{143}Nd/^{144}Nd$ ratios (**Supplementary Figure S2**) (Hoinkes et al., 1997; Thöni and Miller, 2004) compared to other Eastern Alpine nappe systems with a Variscan metamorphic imprint (Thöni and Miller, 2000; Schuster et al., 2001; Habler et al., 2006). The more negative values from the LM and IM apatites are in line with published data from the metasediments and metamagmatites from the Koralpe-Wölz and Drauzug-Gurktal Nappe systems (Thöni and Miller, 2000; Schuster et al., 2001; Habler et al., 2006; Heinrichs et al., 2012).

However, the apatite Sm-Nd isotopic dataset also highlights limitations of the apatite trace-element discrimination diagram used here. Eight out of the ten UM apatites have εNd below −5 (**Figure 5**), which is an unusual low value for Eastern Alpine ultramafic rocks (Thöni and Jagoutz, 1993; Schulz et al., 2004; Habler et al., 2006). The most likely explanation for this mismatch between the geochemical classification and the isotopic composition is a misclassification of the grains by the discrimination diagram. However, as these grains only make up a small share in the apatites population (10 of 406), this misclassification does not interfere with the interpretation.

In summary, the two analyzed grain-size fractions reveal significant differences when provenance changes are recorded, implying that the fractions are recording different information (**Figure 5, 6**). The sand-sized apatite single-grain distributions record the exposure of the new Upper Austroalpine source with higher εNd values as a changing provenance at 23.3 Ma. However, the clay-sized bulk-rock εNd values reveal stable conditions at that time. Vice versa, the clay-sized bulk-rock analysis indicates a provenance change at 19 Ma, when the sand-sized apatites suggest stable conditions. Between 23.3 and 19 Ma the sand-sized apatites and the clay-sized bulk-rock record significantly different provenance information. As both εNd provenance records evolve into less negative values, both records may be governed by the same process: the exposure of the new Upper Austroalpine source with higher εNd values driven by exhumation of the Tauern Window.

Comparison of Total Signal-Lag Times Between Grain-Size Fractions in Response to Tauern Window Exhumation

A difference in the timing of signal arrival between grain-size fractions has been described above. However, contrary to the hypothesis posed by Tofelde et al. (2021), where an environmental signal may be first recorded in the fine-grained sediment fraction due to rapid sediment transport as suspended load, the provenance change is first recorded in the sand-sized apatites; the clay-sized fraction potentially does not show the same provenance shift until 4–5.3 Myrs later. The total signal-lag time [*sensu* Tofelde et al. (2021)], the time span from the onset of the early Tauern Window exhumation to the recording of the provenance change in the sand-sized apatite single-grain distributions, amounts to 3.4–6.0 Myrs (**Figure 3**). The total signal-lag time of the clay-sized bulk-rock εNd values in response to the Tauern Window exhumation is 8.0–10.3 Myrs (**Figure 3**). Hence, the exposure of

the new Upper Austroalpine source with higher εNd values was recorded 4–5.3 Myrs later in the clay-sized fraction than in the sand-sized apatites (**Figure 3**), only after a major reconfiguration of the drainage system reduced the drainage area that provided sediment to the study area by ~60% (**Figure 7**).

The described difference in total signal-lag times (*sensu* Tofelde et al. (2021)) of provenance changes between different grain-size fractions creates challenges and opportunities for our understanding of SRS evolution. Often the sand-sized and/or coarse silt-sized fraction is analyzed for provenance reconstructions of a SRS (e.g., Huber et al., 2018; Morton, 1985; Van Andel, 1950). As highlighted here, their provenance information might significantly differ from other grain-size fractions at least temporarily (**Figure 3**), posing uncertainties on the reliability or completeness of such reconstructions and related sediment-budget calculations (Kuhlemann, 2000).

We regard methodological characteristics in combination with the reconfiguration of the drainage system at 19 Ma to be responsible for the delayed recording of provenance changes. As single-grain analyses provide specific source-rock information from the investigated grains, this single-grain information in the sink can be (in a best-case scenario) directly linked to a specific source (Mange-Rajetzky and Oberhänsli, 1982; Morton, 1985; von Eynatten and Dunkl, 2012). Furthermore, single-grain distributions are often biased towards sources with high mineral fertility and erosion rates which leads to a dominance of these sources in the sink samples, even though those sources are geographically small (Gemignani et al., 2017; Malusà et al., 2017). For a reliable source-to-sink reconstruction, a sufficiently large single-grain population is required (Vermeesch, 2004). In contrast, bulk-rock analytical methods represent a mixture of the entire SRS by integrating over the catchment upstream of the sampled location; information about specific sources can only be gained if results are unmixed (Dickinson, 1985; Roser and Korsch, 1986; Ingersoll, 1990). The resulting provenance information is more comprehensive but less specific than single-grain information. The mixture leads to a dilution of extreme values in e.g., geochemistry, erosion rates, or isotopic ratios from small source areas in the course of the SRS and this extreme endmember information does not reach the sink (Wittmann et al., 2016; Awasthi et al., 2018; Malkowski et al., 2019). Only large-scale changes (e.g., large-scale drainage reorganizations or climatic change) in an orogen-wide SRSs influence the bulk-rock composition of the sedimentary archive in the sink (Clift and Giosan, 2014; Fildani et al., 2018).

In this study, exhumation of the geographically small (~3,125 km^2, Favaro et al. (2017)) but proximal sediment source above the future Tauern Window, with two to six times higher exhumation rates compared to the remaining Eastern Alps (Frisch et al., 2000; Hülscher et al., 2021; Kuhlemann, 2007), changed the apatite single-grain distribution in the sedimentary sink at 23.3 Ma (**Figure 5**). Coarser grain-size fractions tend to be biased towards more proximal sources (Gemignani et al., 2019; Hülscher et al., 2018). However, the Upper Austroalpine source area above the future Tauern Window, which had higher εNd values, was too small to change the clay-sized bulk-rock εNd values in the sink at 23.3 Ma (**Figure 6**). The signal was diluted by the overwhelming

contributions from the remaining sources, especially by the Munich SRS, which was rich in silt and clay (Füchtbauer, 1964; Füchtbauer, 1967). The relative proportion of the area above the future Tauern Window represents ~3% of the entire Chattian/Aquitanian Upper Austrian NAFB source area (**Figure 7**). The tectonically induced (Zweigel, 1998) cut-off of the Munich SRS (Füchtbauer, 1967) at 19 Ma reduced the Upper Austrian Molasse catchment area (**Figure 7**); thereby increasing the relative share of the source area above the future Tauern Window to ~8%. Only this reduction had a large-enough effect to allow the provenance change to be recognizable in the bulk-rock clay-sized εNd values (**Figure 6**). However, as revealed by the apatite single-grain distribution, the provenance change was recorded the Upper Austrian NAFB 4–5.3 Myrs earlier (**Figure 3**).

The differences between signals obtained using single-grain and bulk-rock methods can emphasize information about the extent of a perturbated area in an SRS. As described above, it requires spatially extensive environmental perturbations in a SRS to change the bulk-rock provenance of the sink, but only small-scale environmental perturbations to change the single-grain distribution of the sedimentary sink. In this study, the small-scale exhumation of a late Variscan high-grade metamorphic source rock with higher εNd values above the future Tauern Window was recognizable in the Upper Austrian apatite distribution, but only the large-scale reorganization of the SRSs made it recognizable in the bulk-rock clay-sized εNd values. However, processes that affect larger parts of an SRS have been reported to change bulk-rock and single-grain methods simultaneously (Clift and Giosan, 2014; Bracciali et al., 2015; Fildani et al., 2018). These processes include climatic perturbations such as a changing erosional focus (Clift and Giosan, 2014) or drainage reorganization (Fildani et al., 2018) but also tectonic perturbations triggering large-scale drainage reorganizations (Bracciali et al., 2015). However, tectonic exhumation processes interfere only with segments of an orogen-wide SRS and related provenance changes are driven by the exposure of a new source rock (Brügel et al., 2003; Anfinson et al., 2020) or a drainage-divide migration caused by surface uplift (Mark et al., 2016; Lu et al., 2019). Taking these ideas further, by combining single-grain and bulk-rock approaches, provenance changes driven by tectonic exhumation processes from those driven by large-scale processes may be distinguished just from their imprint in the sedimentary sink. This enables a previously unattained understanding of the underlying environmental change, especially for ancient SRSs where independent constrains are missing.

CONCLUSION

In this study, the clay-sized and sand-sized fractions of the Chattian to Burdigalian infill of the Upper Austrian Northern Alpine Foreland Basin (NAFB) have been analyzed for provenance signals. A previously published multi-proxy single-grain analysis of sand-sized apatites (trace-element geochemistry, fission track, and U-Pb ages (Hülscher et al., 2021)) was expanded by the Sm-Nd isotopic composition of the same apatites and revealed a provenance change at 23.3 ± 0.3 Ma governed by the exhumation of a late Variscan high-grade metamorphic source rock with increased εNd values above the future Tauern Window in the Eastern Alps. In

contrast, the clay-sized bulk-rock Nd isotope analyses suggests a stable provenance from ~27 to 19 Ma, dominated by input from the German and Swiss NAFB, which was rich in fine-grained (<63 μm) material originally sourced from the Central Alps (Füchtbauer, 1964, 1967). This source was cut off from the Upper Austrian NAFB at 19 Ma during a major rearrangement of the SRSs in the entire NAFB, which turned the Upper Austrian NAFB from a marine transfer zone to a terminal sink, resulting in a reduction of the Upper Austrian NAFB source area and a relative increase in Eastern Alpine sources. The clay-sized bulk-rock εNd values after 19 Ma are too unspecific to connect them to a specific Eastern Alpine source; however, in connection with the apatite single-grain information, they may be interpreted as sediments with a provenance from the same late Variscan high-grade metamorphic source rock with higher εNd values. Therefore, the clay-sized sediments in the Upper Austrian NAFB are interpreted as recording the provenance change after 19 Ma and 4–5 Myrs later then in the sand-sized fraction. This selective recording of the tectonic forcing from the hinterland in the sediment record is controlled by the dilution and concentration of the signal in the bulk-rock clay-size fraction and sand-sized single-grain analysis, respectively.

By quantifying total signal-lag times of sedimentary provenance changes using different methods, valuable information about the underlying perturbation is gained as the different methods emphasize or de-emphasize different aspects of the same process. In the presented study, the small area of the newly exposed source rocks is likely to explain the delay of the area-averaged εNd signal in the clay-sized sediment fraction. However, a process affecting large parts of a source area is likely to contemporaneously change the single-grain distribution and bulk-rock geochemistry in the sedimentary archive. Such a contemporaneous provenance change has been described in response to Holocene climate change (Clift and Giosan, 2014; Fildani et al., 2018). Obtaining information about the areal extent of a perturbation affecting a sediment routing system by provenance analysis holds great potential to gain insights about the forcing mechanism of environmental changes in ancient sediment routing systems.

DATA AVAILABILITY STATEMENT

The original contributions presented in the study are included in the article/**Supplementary Material**, further inquiries can be directed to the corresponding author.

AUTHOR CONTRIBUTIONS

JH sampled the drill cores and well cuttings and prepared the apatite samples together with ES. NK prepared the well cutting samples and conducted the chemical Nd separation under the supervision of JEH. IM analyzed the apatites for their Sm-Nd isotopic composition. KH conducted the Monte-Carlo simulation of the clay-sized bulk-rock Nd isotopic results. JH wrote the manuscript which benefited greatly from the suggestions of all co-authors. AB, ES, and JH developed the project idea, interpretations, and designed the manuscript under JH's lead.

FUNDING

ACKNOWLEDGMENTS

SUPPLEMENTARY MATERIAL

The Supplementary Material for this article can be found online at: https://www.frontiersin.org/articles/10.3389/feart.2022.914409/full#supplementary-material

REFERENCES

Agnini, C., Fornaciari, E., Raffi, I., Catanzariti, R., Pälike, H., Backman, J., et al. (2014). Biozonation and Biochronology of Paleogene Calcareous Nannofossils from Low and Middle Latitudes. *Newsletters Stratigr.* 47 (2), 131–181. doi:10.1127/0078-0421/2014/0042

Anfinson, O. A., Stockli, D. F., Miller, J. C., Möller, A., and Schlunegger, F. (2020). Tectonic Exhumation of the Central Alps Recorded by Detrital Zircon in the Molasse Basin, Switzerland. *Solid earth.* 11 (6), 2197–2220. doi:10.5194/se-11-2197-2020

Awasthi, N., Ray, E., and Paul, D. (2018). Sr and Nd Isotope Compositions of Alluvial Sediments from the Ganga Basin and Their Use as Potential Proxies for Source Identification and Apportionment. *Chem. Geol.* 476, 327–339. doi:10.1016/j.chemgeo.2017.11.029

Backman, J., Raffi, I., Rio, D., Fornaciari, E., and Pälike, H. (2012). Biozonation and Biochronology of Miocene through Pleistocene Calcareous Nannofossils from Low and Middle Latitudes. *Newsletters Stratigr.* 45 (3), 221–244. doi:10.1127/0078-0421/2012/0022

Belousova, E. A., Griffin, W. L., O'Reilly, S. Y., and Fisher, N. I. (2002). Apatite as an Indicator Mineral for Mineral Exploration: Trace-Element Compositions and Their Relationship to Host Rock Type. *J. Geochem. Explor.* 76 (1), 45–69. doi:10.1016/s0375-6742(02)00204-2

Bernhard, F., Klötzli, U., Thöni, M., and Hoinkes, G. (1996). Age, Origin and Geodynamic Significance of a Polymetamorphic Felsic Intrusion in the Ötztal Crystalline Basement. *Tirol, Austria Mineralogy Petrology* 58 (3-4), 171–196. doi:10.1007/bf01172095

Bernhardt, A., Stright, L., and Lowe, D. R. (2012). Channelized Debris-flow Deposits and Their Impact on Turbidity Currents: The Puchkirchen Axial Channel Belt in the Austrian Molasse Basin. *Sedimentology* 59 (7), 2042–2070. doi:10.1111/j.1365-3091.2012.01334.x

Blum, M., Rogers, K., Gleason, J., Najman, Y., Cruz, J., and Fox, L. (2018). Allogenic and Autogenic Signals in the Stratigraphic Record of the Deep-Sea Bengal Fan. *Sci. Rep.* 8 (1), 1–13. doi:10.1038/s41598-018-25819-5

Braccialli, L., Najman, Y., Parrish, R. R., Akhter, S. H., and Millar, I. (2015). The Brahmaputra Tale of Tectonics and Erosion: Early Miocene River Capture in the Eastern Himalaya. *Earth & Planet. Sci. Lett.* 415, 25–37.

Brügel, A., Dunkl, I., Frisch, W., Kuhlemann, J., and Balogh, K. (2000). The Record of Periadriatic Volcanism in the Eastern Alpine Molasse Zone and its Palaeogeographic Implications. *Terra nova.* 12 (1), 42–47. doi:10.1046/j.1365-3121.2000.00269.x

Brügel, A., Dunkl, I., Frisch, W., Kuhlemann, J., and Balogh, K. (2003). Geochemistry and Geochronology of Gneiss Pebbles from Foreland Molasse Conglomerates: Geodynamic and Paleogeographic Implications for the Oligo-Miocene Evolution of the Eastern Alps. *J. Geol.* 111 (5), 543–563. doi:10.1086/376765

Chew, D. M., Petrus, J. A., and Kamber, B. S. (2014). U-pb LA-ICPMS Dating Using Accessory Mineral Standards with Variable Common Pb. *Chem. Geol.* 363, 185–199. doi:10.1016/j.chemgeo.2013.11.006

Clift, P. D., and Giosan, L. (2014). Sediment Fluxes and Buffering in the Post-glacial Indus Basin. *Basin Res.* 26 (3), 369–386. doi:10.1111/bre.12038

Clift, R. A., Droop, G. T. R., and Rex, D. C. (1985). Alpine Metamorphism in the South-East Tauern Window, Austria: 2. Rates of Heating, Cooling and Uplift. *J. Metamorph Geol.* 3 (4), 403–415. doi:10.1111/j.1525-1314.1985.tb00327.x

Clift, P. D., Hodges, K. V., Heslop, D., Hannigan, R., Van Long, H., and Calves, G. (2008). Correlation of Himalayan Exhumation Rates and Asian Monsoon Intensity. *Nat. Geosci.* 1 (12), 875–880. doi:10.1038/ngeo351

Covault, J. A., Hubbard, S. M., Graham, S. A., Hinsch, R., and Linzer, H.-G. (2009). Turbidite-reservoir Architecture in Complex Foredeep-Margin and Wedge-Top Depocenters, Tertiary Molasse Foreland Basin System, Austria. *Mar. Petroleum Geol.* 26 (3), 379–396. doi:10.1016/j.marpetgeo.2008.03.002

De Ruig, M. J., and Hubbard, S. M. (2006). Seismic Facies and Reservoir Characteristics of a Deep-Marine Channel Belt in the Molasse Foreland Basin, Puchkirchen Formation, Austria. *AAPG Bull.* 90 (5), 735–752. doi:10.1306/10210505018

DePaolo, D. J., and Wasserburg, G. J. (1976). Nd Isotopic Variations and Petrogenetic Models. *Geophys. Res. Lett.* 3 (5), 249–252. doi:10.1029/gl003i005p00249

Dickinson, W. R. (1985). "Interpreting Provenance Relations from Detrital Modes of Sandstones," in *Provenance of Arenites* (Springer), 333–361. doi:10.1007/978-94-017-2809-6_15

Dill, H. (1994). Can REE Patterns and U-Th Variations Be Used as a Tool to Determine the Origin of Apatite in Clastic Rocks? *Sediment. Geol.* 92 (3-4), 175–196. doi:10.1016/0037-0738(94)90105-8

Dunkl, I., Frisch, W., Kuhlemann, J., and Brügel, A. (2009). Pebble Population Dating as an Additional Tool for Provenance Studies - Examples from the Eastern Alps. *Geol. Soc. Lond. Spec. Publ.* 324 (1), 125–140. doi:10.1144/sp324.10

Favaro, S., Schuster, R., Handy, M. R., Scharf, A., and Pestal, G. (2015). Transition from Orogen-Perpendicular to Orogen-Parallel Exhumation and Cooling during Crustal Indentation - Key Constraints from 147Sm/144Nd and 87Rb/87Sr Geochronology (Tauern Window, Alps). *Tectonophysics* 665, 1–16. doi:10.1016/j.tecto.2015.08.037

Favaro, S., Handy, M. R., Scharf, A., and Schuster, R. (2017). Changing Patterns of Exhumation and Denudation in Front of an Advancing Crustal Indenter, Tauern Window (Eastern Alps). *Tectonics* 36 (6), 1053–1071. doi:10.1002/2016tc004448

Fildani, A., Hessler, A. M., Mason, C. C., McKay, M. P., and Stockli, D. F. (2018). Late Pleistocene Glacial Transitions in North America Altered Major River Drainages, as Revealed by Deep-Sea Sediment. *Sci. Rep.* 8 (1), 1–8. doi:10.1038/s41598-018-32268-7

Filek, T., Hofmayer, F., Feichtinger, I., Berning, B., Pollerspöck, J., Zwicker, J., et al. (2021). Environmental Conditions during the Late Oligocene Transgression in the North Alpine Foreland Basin (Eferding Formation, Egerian) - A Multidisciplinary Approach. *Palaeogeogr. Palaeoclimatol. Palaeoecol.* 580, 110527. doi:10.1016/j.palaeo.2021.110527

Finger, F., Roberts, M., Haunschmid, B., Schermaier, A., and Steyrer, H. (1997). Variscan Granitoids of Central Europe: Their Typology, Potential Sources and Tectonothermal Relations. *Mineralogy Petrology* 61 (1-4), 67–96. doi:10.1007/bf01172478

Foster, G., and Carter, A. (2007). Insights into the Patterns and Locations of Erosion in the Himalaya—A Combined Fission-Track and *In Situ* Sm–Nd Isotopic Study of Detrital Apatite. *Earth Planet. Sci. Lett.* 257 (3-4), 407–418. doi:10.1016/j.epsl.2007.02.044

Foster, G. L., and Vance, D. (2006). *In Situ* Nd Isotopic Analysis of Geological Materials by Laser Ablation MC-ICP-MS. *J. Anal. At. Spectrom.* 21 (3), 288–296. doi:10.1039/b513945g

Frisch, W., Dunkl, I., and Kuhlemann, J. (2000). Post-collisional Orogen-Parallel Large-Scale Extension in the Eastern Alps. *Tectonophysics* 327 (3), 239–265. doi:10.1016/s0040-1951(00)00204-3

Frisch, W., Kuhlemann, J., Dunkl, I., and Székely, B. (2001). The Dachstein Paleosurface and the Augenstein Formation in the Northern Calcareous Alps - a Mosaic Stone in the Geomorphological Evolution of the Eastern Alps. *Int. J. Earth Sci.* 90 (3), 500–518. doi:10.1007/s005310000189

Füchtbauer, H. (1964). *Sedimentpetrographische Untersuchungen in der älteren Molasse nördlich der Alpen*, 57. Eclogae Geologicae Helvetiae.

Füchtbauer, H. (1967). Die Sandsteine in der Molasse nördlich der Alpen. *Geol. Rundsch.* 56 (1), 266–300. doi:10.1007/bf01848720

Garçon, M., Chauvel, C., France-Lanord, C., Huyghe, P., and Lavé, J. (2013). Continental Sedimentary Processes Decouple Nd and Hf Isotopes. *Geochimica Cosmochimica Acta* 121, 177–195. doi:10.1016/j.gca.2013.07.027

Garçon, M., Boyet, M., Carlson, R. W., Horan, M. F., Auclair, D., and Mock, T. D. (2018). Factors Influencing the Precision and Accuracy of Nd Isotope Measurements by Thermal Ionization Mass Spectrometry. *Chem. Geol.* 476, 493–514. doi:10.1016/j.chemgeo.2017.12.003

Garefalakis, P., and Schlunegger, F. (2019). Tectonic Processes, Variations in Sediment Flux, and Eustatic Sea Level Recorded by the 20 Myr Old Burdigalian Transgression in the Swiss Molasse Basin. *Solid earth.* 10 (6), 2045–2072. doi:10.5194/se-10-2045-2019

Garver, J. I., Brandon, M. T., Roden-Tice, M., and Kamp, P. J. J. (1999). Exhumation History of Orogenic Highlands Determined by Detrital Fission-Track Thermochronology. *Geol. Soc. Lond. Spec. Publ.* 154 (1), 283–304. doi:10.1144/gsl.sp.1999.154.01.13

Gemignani, L., Kuiper, K. F., Wijbrans, J. R., Sun, X., and Santato, A. (2019). Improving the Precision of Single Grain Mica 40Ar/39Ar-Dating on Smaller and Younger Muscovite Grains: Application to Provenance Studies. *Chem. Geol.* 511, 100–111. doi:10.1016/j.chemgeo.2019.02.013

Gemignani, L., Sun, X., Braun, J., Gerve, T., and Wijbrans, J. R. (2017). A New Detrital Mica 40Ar/39Ar Dating Approach for Provenance and Exhumation of the Eastern Alps. *Tectonics* 36, 1521–1537. doi:10.1002/2017tc004483

Gier, S. (1998). Burial Diagenetic Processes and Clay Mineral Formation in the Molasse Zone of Upper Austria. *Clays clay minerals* 46 (6), 658–669. doi:10.1346/ccmn.1998.0460606

Gleadow, A. J. W., and Lovering, J. F. (1974). The Effect of Weathering on Fission Track Dating. *Earth Planet. Sci. Lett.* 22 (2), 163–168. doi:10.1016/0012-821x(74)90077-6

Goldstein, S. J., and Jacobsen, S. B. (1988). Nd and Sr Isotopic Systematics of River Water Suspended Material: Implications for Crustal Evolution. *Earth Planet. Sci. Lett.* 87 (3), 249–265. doi:10.1016/0012-821x(88)90013-1

Goldstein, S. L., and Hemming, S. R. (2003). Long-lived Isotopic Tracers in Oceanography, Paleoceanography, and Ice-Sheet Dynamics. *Treatise Geochem.* 6, 625. doi:10.1016/b0-08-043751-6/06179-x

Goldstein, S. L., O'nions, R. K., and Hamilton, P. J. (1984). A Sm-Nd Isotopic Study of Atmospheric Dusts and Particulates from Major River Systems. *Earth Planet. Sci. Lett.* 70 (2), 221–236. doi:10.1016/0012-821x(84)90007-4

Gradstein, F., Ogg, J., Schmitz, M., and Ogg, G. (2012). *The Geologic Time Scale 2012.* Amsrerdam: Elsevier, 1176.

Grundtner, M.-L., Gross, D., Linzer, H. G., Neuhuber, S., Sachsenhofer, R. F., and Scheucher, L. (2016). The Diagenetic History of Oligocene-Miocene Sandstones of the Austrian North Alpine Foreland Basin. *Mar. Petroleum Geol.* 77, 418–434. doi:10.1016/j.marpetgeo.2016.04.003

Grunert, P., Hinsch, R., Sachsenhofer, R. F., Bechtel, A., Ćorić, S., Harzhauser, M., et al. (2013). Early Burdigalian Infill of the Puchkirchen Trough (North Alpine Foreland Basin, Central Paratethys): Facies Development and Sequence Stratigraphy. *Mar. Petroleum Geol.* 39 (1), 164–186. doi:10.1016/j.marpetgeo.2012.08.009

Grunert, P., Tzanova, A., Harzhauser, M., and Piller, W. E. (2014). Mid-Burdigalian Paratethyan Alkenone Record Reveals Link between Orbital Forcing, Antarctic Ice-Sheet Dynamics and European Climate at the Verge to Miocene Climate Optimum. *Glob. Planet. Change* 123, 36–43. doi:10.1016/j.gloplacha.2014.10.011

Grunert, P., Auer, G., Harzhauser, M., and Piller, W. E. (2015). Stratigraphic Constraints for the Upper Oligocene to Lower Miocene Puchkirchen Group (North Alpine Foreland Basin, Central Paratethys). *Newsletters Stratigr.* 48 (1), 111–133. doi:10.1127/nos/2014/0056

Habler, G., Thöni, M., and Sölva, H. (2006). Tracing the High Pressure Stage in the Polymetamorphic Texel Complex (Austroalpine Basement Unit, Eastern Alps): P–T–T–D Constraints. *Mineralogy Petrology* 88 (1-2), 269–296. doi:10.1007/s00710-006-0143-7

Habler, G., Thöni, M., and Miller, C. (2007). Major and Trace Element Chemistry and Sm–Nd Age Correlation of Magmatic Pegmatite Garnet Overprinted by Eclogite-Facies Metamorphism. *Chem. Geol.* 241 (1-2), 4–22. doi:10.1016/j.chemgeo.2007.01.026

Habler, G., Thöni, M., and Grasemann, B. (2009). Cretaceous Metamorphism in the Austroalpine Matsch Unit (Eastern Alps): the Interrelation between Deformation and Chemical Equilibration Processes. *Mineralogy Petrology* 97 (3-4), 149. doi:10.1007/s00710-009-0094-x

Heinrichs, T., Siegesmund, S., Frei, D., Drobe, M., and Schulz, B. (2012). Provenance Signatures from Whole-Rock Geochemistry and Detrital Zircon Ages of Metasediments from the Austroalpine Basement South of the Tauern Window (Eastern Tyrol, Austria). *Geo Alp.* 9, 156–185.

Henrichs, I. A., O'Sullivan, G., Chew, D., Mark, C., Babechuk, M. G., McKenna, C., et al. (2018). The Trace Element and U-Pb Systematics of Metamorphic Apatite. *Chem. Geol.* 483, 218–238. doi:10.1016/j.chemgeo.2017.12.031

Henry, P., Deloule, E., and Michard, A. (1997). The Erosion of the Alps: Nd Isotopic and Geochemical Constraints on the Sources of the Peri-Alpine Molasse Sediments. *Earth Planet. Sci. Lett.* 146 (3-4), 627–644. doi:10.1016/s0012-821x(96)00252-x

Hinsch, R. (2008). New Insights into the Oligocene to Miocene Geological Evolution of the Molasse Basin of Austria. *OIL GAS-EUROPEAN Mag.* 34 (3), 138–143.

Hodges, J. L. (1958). The Significance Probability of the Smirnov Two-Sample Test. *Ark. Mat.* 3 (5), 469–486. doi:10.1007/bf02589501

Hoinkes, G., Thöni, M., Lichem, C., Bernhard, F., Kaindl, R., Schweigl, J., et al. (1997). Metagranitoids and Associated Metasediments as Indicators for the Pre-Alpine Magmatic and Metamorphic Evolution of the Western Austroalpine Ötztal Basement (Kaunertal, Tirol). *Schweiz Mineral. Petrogr. Mitt* 77, 299–314. doi:10.5169/seals-58486

Hubbard, S. M., de Ruig, M. J., and Graham, S. A. (2009). Confined Channel-Levee Complex Development in an Elongate Depo-Center: Deep-Water Tertiary Strata of the Austrian Molasse Basin. *Mar. Petroleum Geol.* 26 (1), 85–112. doi:10.1016/j.marpetgeo.2007.11.006

Huber, B., Bahlburg, H., Berndt, J., Dunkl, I., and Gerdes, A. (2018). Provenance of the Surveyor Fan and Precursor Sediments in the Gulf of Alaska-Implications of a Combined U-Pb, (U-Th)/He, Hf, and Rare Earth Element Study of Detrital Zircons. *J.* 126 (6), 577–600. doi:10.1086/699740

Hülscher, J., Bahlburg, H., and Pfänder, J. (2018). New Geochemical Results Indicate a Non-alpine Provenance for the Alpine Spectrum (Epidote, Garnet, Hornblende) in Quaternary Upper Rhine Sediment. *Sediment. Geol.* 375, 134–144. doi:10.1016/j.sedgeo.2018.02.010

Hülscher, J., Fischer, G., Grunert, P., Auer, G., and Bernhardt, A. (2019). Selective Recording of Tectonic Forcings in an Oligocene/Miocene Submarine Channel System: Insights from New Age Constraints and Sediment Volumes from the Austrian Northern Alpine Foreland Basin. *Front. Earth Sci.* 7–302. doi:10.3389/feart.2019.00302

Hülscher, J., Sobel, E. R., Verwater, V., Groß, P., Chew, D., and Bernhardt, A. (2021). Detrital Apatite Geochemistry and Thermochronology from the Oligocene/Miocene Alpine Foreland Record the Early Exhumation of the Tauern Window. *Basin Res.* 33, 3021–3044. doi:10.1111/bre.12593

Ingersoll, R. V. (1990). Actualistic Sandstone Petrofacies: Discriminating Modern and Ancient Source Rocks. *Geol* 18 (8), 733–736. doi:10.1130/0091-7613(1990)018<0733:aspdma>2.3.co;2

Jacobsen, S. B., and Wasserburg, G. J. (1980). Sm-Nd Isotopic Evolution of Chondrites. *Earth Planet. Sci. Lett.* 50 (1), 139–155. doi:10.1016/0012-821x(80)90125-9

Jerolmack, D. J., and Paola, C. (2010). Shredding of Environmental Signals by Sediment Transport. *Geophys. Res. Lett.* 37–19. doi:10.1029/2010gl044638

Jonell, T. N., Li, Y., Blusztajn, J., Giosan, L., and Clift, P. D. (2018). Signal or Noise? Isolating Grain Size Effects on Nd and Sr Isotope Variability in Indus Delta Sediment Provenance. *Chem. Geol.* 485, 56–73. doi:10.1016/j.chemgeo.2018.03.036

Kremer, C. H., McHargue, T., Scheucher, L., and Graham, S. A. (2018). Transversely-sourced Mass-Transport Deposits and Stratigraphic Evolution

of a Foreland Submarine Channel System: Deep-Water Tertiary Strata of the Austrian Molasse Basin. *Mar. Petroleum Geol.* 92, 1–19. doi:10.1016/j.marpetgeo.2018.01.035

Kuhlemann, J., Dunkl, I., Brügel, A., Spiegel, C., and Frisch, W. (2006). From Source Terrains of the Eastern Alps to the Molasse Basin: Detrital Record of Non-steady-state Exhumation. *Tectonophysics* 413 (3), 301–316. doi:10.1016/j.tecto.2005.11.007

Kuhlemann, J., and Kempf, O. (2002). Post-eocene Evolution of the North Alpine Foreland Basin and its Response to Alpine Tectonics. *Sediment. Geol.* 152 (1), 45–78. doi:10.1016/s0037-0738(01)00285-8

Kuhlemann, J. (2007). Paleogeographic and Paleotopographic Evolution of the Swiss and Eastern Alps since the Oligocene. *Glob. Planet. Change* 58 (1), 224–236. doi:10.1016/j.gloplacha.2007.03.007

Kuhlemann, J. (2000). Post-collisional Sediment Budget of Circum-Alpine Basins (Central Europe). *Mem. Sci. Geol. Padova* 52 (1), 1–91.

Liew, T. C., and Hofmann, A. W. (1988). Precambrian Crustal Components, Plutonic Associations, Plate Environment of the Hercynian Fold Belt of Central Europe: Indications from a Nd and Sr Isotopic Study. *Contrib. Mineral. Pet.* 98 (2), 129–138. doi:10.1007/bf00402106

Lu, G., Di Capua, A., Winkler, W., Rahn, M., Guillong, M., von Quadt, A., et al. (2019). Restoring the Source-To-Sink Relationships in the Paleogene Foreland Basins in the Central and Southern Alps (Switzerland, Italy, France): a Detrital Zircon Study Approach. *Int. J. Earth Sci. Geol. Rundsch)* 108 (6), 1817–1834. doi:10.1007/s00531-019-01734-6

Malkowski, M. A., Sharman, G. R., Johnstone, S. A., Grove, M. J., Kimbrough, D. L., and Graham, S. A. (2019). Dilution and Propagation of Provenance Trends in Sand and Mud: Geochemistry and Detrital Zircon Geochronology of Modern Sediment from Central California (U.S.A.). *Am. J. Sci.* 319 (10), 846–902. doi:10.2475/10.2019.02

Malusà, M. G., Wang, J., Garzanti, E., Liu, Z.-C., Villa, I. M., and Wittmann, H. (2017). Trace-element and Nd-Isotope Systematics in Detrital Apatite of the Po River Catchment: Implications for Provenance Discrimination and the Lag-Time Approach to Detrital Thermochronology. *Lithos* 290, 48–59. doi:10.1016/j.lithos.2017.08.006

Mange-Rajetzky, M., and Oberhänsli, R. (1982). Detrital Lawsonite and Blue Sodic Amphibole in the Molasse of Savoy, France and Their Significance in Assessing Alpine Evolution. *Schweiz. Mineral. Petrogr. Mittl.* 62, 415–436. doi:10.5169/seals-47979

Mark, C., Cogné, N., and Chew, D. (2016). Tracking Exhumation and Drainage Divide Migration of the Western Alps: A Test of the Apatite U-Pb Thermochronometer as a Detrital Provenance Tool. *Bulletin* 128 (9-10), 1439–1460. doi:10.1130/b31351.1

Masalimova, L. U., Lowe, D. R., Mchargue, T., and Derksen, R. (2015). Interplay between an Axial Channel Belt, Slope Gullies and Overbank Deposition in the Puchkirchen Formation in the Molasse Basin, Austria. *Sedimentology* 62 (6), 1717–1748. doi:10.1111/sed.12201

McCulloch, M. T., and Wasserburg, G. J. (1978). Sm-Nd and Rb-Sr Chronology of Continental Crust Formation. *Science* 200 (4345), 1003–1011. doi:10.1126/science.200.4345.1003

Morton, A. C. (1985). A New Approach to Provenance Studies: Electron Microprobe Analysis of Detrital Garnets from Middle Jurassic Sandstones of the Northern North Sea. *Sedimentology* 32 (4), 553–566. doi:10.1111/j.1365-3091.1985.tb00470.x

Morton, A., and Yaxley, G. (2007). Detrital Apatite Geochemistry and its Application in Provenance Studies. *SPECIAL PAPERS-GEOLOGICAL Soc. Am.* 420, 319. doi:10.1130/2006.2420(19)

Mosbrugger, V., Utescher, T., and Dilcher, D. L. (2005). Cenozoic Continental Climatic Evolution of Central Europe. *Proc. Natl. Acad. Sci. U.S.A.* 102 (42), 14964–14969. doi:10.1073/pnas.0505267102

Murray, A. B., Lazarus, E., Ashton, A., Baas, A., Coco, G., Coulthard, T., et al. (2009). Geomorphology, Complexity, and the Emerging Science of the Earth's Surface. *Geomorphology* 103 (3), 496–505. doi:10.1016/j.geomorph.2008.08.013

O'Sullivan, G. J., Chew, D. M., Morton, A. C., Mark, C., and Henrichs, I. A. (2018). An Integrated Apatite Geochronology and Geochemistry Tool for Sedimentary Provenance Analysis. *Geochem. Geophys. Geosyst.* 19 (4), 1309–1326. doi:10.1002/2017gc007343

O'Sullivan, G., Chew, D., Kenny, G., Henrichs, I., and Mulligan, D. (2020). The Trace Element Composition of Apatite and its Application to Detrital Provenance Studies. *Earth-Science Rev.* 201, 103044. doi:10.1016/j.earscirev.2019.103044

Ortner, H., and Stingl, V. (2001). *Facies and basin development of the Oligocene in the Lower Inn Valley, Tyrol/Bavaria, Wien, Österreichische Akademie der Wissenschaften, Schriftreihe der Erdwissenschaftlichen Kommision*. in *Paleogene of the Eastern Alps*, 14.

Paton, C., Hellstrom, J., Paul, B., Woodhead, J., and Hergt, J. (2011). Iolite: Freeware for the Visualisation and Processing of Mass Spectrometric Data. *J. Anal. At. Spectrom.* 26 (12), 2508–2518. doi:10.1039/c1ja10172b

Piller, W. E., Harzhauser, M., and Mandic, O. (2007). Miocene Central Paratethys Stratigraphy–Current Status and Future Directions. *Stratigraphy* 4, 151–168.

Platt, N. H., and Keller, B. (1992). Distal Alluvial Deposits in a Foreland Basin Setting-The Lower Freshwater Miocene), Switzerland: Sedimentology, Architecture and Palaeosols. *Sedimentology* 39 (4), 545–565. doi:10.1111/j.1365-3091.1992.tb02136.x

R Core Team (2020). *R: A Language and Environment for Statistical Computing*.

Reddy, S., Cliff, R., and East, R. (1993). Thermal History of the Sonnblick Dome, South-East Tauern Window, Austria: Implications for Heterogeneous Uplift within the Pennine Basement. *Geol. Rundsch.* 82 (4), 667–675. doi:10.1007/bf00191494

Richard, P., Shimizu, N., and Allègre, C. J. (1976). 143Nd/146Nd, a Natural Tracer: an Application to Oceanic Basalts. *Earth Planet. Sci. Lett.* 31 (2), 269–278. doi:10.1016/0012-821x(76)90219-3

Rode, S., Rösel, D., and Schulz, B. (2012). Constraints on the Variscan P-T Evolution by EMP Th-U-Pb Monazite Dating in the Polymetamorphic Austroalpine Oetztal-Stubai Basement (Eastern Alps). *Z. Dtsch. Ges. für Geowiss.* 163 (1), 43–67. doi:10.1127/1860-1804/2012/0163-0043

Rögl, F., Hochuli, P., and Muller, C. (1979). Oligocene–early Miocene stratigraphic correlations in the Molasse Basin of Austria: Annales Geologiques des Pays Helleniques. *Tome Hors Ser.* 30, 1045–1050.

Romans, B. W., Castelltort, S., Covault, J. A., Fildani, A., and Walsh, J. P. (2016). Environmental Signal Propagation in Sedimentary Systems across Timescales. *Earth-Science Rev.* 153, 7–29. doi:10.1016/j.earscirev.2015.07.012

Roser, B. P., and Korsch, R. J. (1986). Determination of Tectonic Setting of Sandstone-Mudstone Suites Using SiO2 Content and K2O/Na2O Ratio. *J. Geol.* 94 (5), 635–650. doi:10.1086/629071

Scharf, A., Handy, M. R., Ziemann, M. A., and Schmid, S. M. (2013). Peak-temperature Patterns of Polyphase Metamorphism Resulting from Accretion, Subduction and Collision (Eastern Tauern Window, European Alps) - a Study with Raman Microspectroscopy on Carbonaceous Material (RSCM). *J. Meta. Geol.* 31 (8), 863–880. doi:10.1111/jmg.12048

Schlunegger, F., and Castelltort, S. (2016). Immediate and Delayed Signal of Slab Breakoff in Oligo/Miocene Molasse Deposits from the European Alps. *Sci. Rep.* 6, 31010. doi:10.1038/srep31010

Schmid, S. M., Fügenschuh, B., Kissling, E., and Schuster, R. (2004). Tectonic Map and Overall Architecture of the Alpine Orogen. *Eclogae Geol. Helv.* 97 (1), 93–117. doi:10.1007/s00015-004-1113-x

Schmid, S. M., Scharf, A., Handy, M. R., and Rosenberg, C. L. (2013). The Tauern Window (Eastern Alps, Austria): a New Tectonic Map, with Cross-Sections and a Tectonometamorphic Synthesis. *Swiss J. Geosci.* 106 (1), 1–32. doi:10.1007/s00015-013-0123-y

Schneider, S., Hammerschmidt, K., Rosenberg, C. L., Gerdes, A., Frei, D., and Bertrand, A. (2015). U-pb Ages of Apatite in the Western Tauern Window (Eastern Alps): Tracing the Onset of Collision-Related Exhumation in the European Plate. *Earth Planet. Sci. Lett.* 418, 53–65. doi:10.1016/j.epsl.2015.02.020

Schulz, B., Bombach, K., Pawlig, S., and Brätz, H. (2004). Neoproterozoic to Early-Palaeozoic Magmatic Evolution in the Gondwana-Derived Austroalpine Basement to the South of the Tauern Window (Eastern Alps). *Int. J. Earth Sci. Geol. Rundsch)* 93 (5), 824–843. doi:10.1007/s00531-004-0421-8

Schulz, H.-M., van Berk, W., Bechtel, A., Struck, U., and Faber, E. (2009). Bacterial Methane in the Atzbach-Schwanenstadt Gas Field (Upper Austrian Molasse Basin), Part I: Geology. *Mar. Petroleum Geol.* 26 (7), 1163–1179. doi:10.1016/j.marpetgeo.2008.12.004

Schulz, B., Krause, J., and Zimmermann, R. (2019). Electron Microprobe Petrochronology of Monazite-Bearing Garnet Micaschists in the Oetztal-

Stubai Complex (Alpeiner Valley, Stubai). *Swiss J. Geosciences* 112 (2-3), 597–617. doi:10.1007/s00015-019-00351-4

Schuster, R., Scharbert, S., Abart, R., and Frank, W. (2001). Permo-Triassic Extension and Related HT/LP Metamorphism in the Austroalpine-Southalpine Realm. *Mitt. Ges. Geol. Bergbaustud. Österr* 45, 111–141.

Sharman, G. R., Hubbard, S. M., Covault, J. A., Hinsch, R., Linzer, H.-G., and Graham, S. A. (2018). Sediment Routing Evolution in the North Alpine Foreland Basin, Austria: Interplay of Transverse and Longitudinal Sediment Dispersal. *Basin Res.* 30, 426–447. doi:10.1111/bre.12259

Sharman, G. R., Sylvester, Z., and Covault, J. A. (2019). Conversion of Tectonic and Climatic Forcings into Records of Sediment Supply and Provenance. *Sci. Rep.* 9 (1), 4115–4117. doi:10.1038/s41598-019-39754-6

Sinclair, H. (1997). Tectonostratigraphic Model for Underfilled Peripheral Foreland Basins: An Alpine Perspective. *Geol. Soc. Am. Bull.* 109 (3), 324–346. doi:10.1130/0016-7606(1997)109<0324:tmfupf>2.3.co;2

Skeries, W., and Georg Troll, G. (1991). "Der Geröllbestand in Molassekonglomeraten des Chiemgaus (Bayern) und seine paläogeographischen Beziehungen zum alpinen Liefergebiet," in *Zeitschrift der deutschen geologischen Gesellschaft*, 43–66. doi:10.1127/zdgg/142/1991/43

Tatzel, M., Dunkl, I., and von Eynatten, H. (2017). Provenance of Palaeo-Rhine Sediments from Zircon Thermochronology, Geochemistry, U/Pb Dating and Heavy Mineral Assemblages. *Basin Res.* 29, 396–417. doi:10.1111/bre.12155

Teipel, U., Eichhorn, R., Loth, G., Rohrmüller, J., Höll, R., and Kennedy, A. (2004). U-pb SHRIMP and Nd Isotopic Data from the Western Bohemian Massif (Bayerischer Wald, Germany): Implications for Upper Vendian and Lower Ordovician Magmatism. *Int. J. Earth Sci. Geol. Rundsch)* 93 (5), 782–801. doi:10.1007/s00531-004-0419-2

Thöni, M. (2006). Dating Eclogite-Facies Metamorphism in the Eastern Alps–Approaches, Results, Interpretations: a Review. *Mineralogy Petrology* 88 (1-2), 123–148. doi:10.1007/s00710-006-0153-5

Thöni, M., and Jagoutz, E. (1993). Isotopic Constraints for Eo-Alpine High-P Metamorphism in the Austroalpine Nappes of the Eastern Alps: Bearing on Alpine Orogenesis. *Schweiz. Mineral. Petrogr. Mittl.* 73 (2), 177–189. doi:10.1016/0016-7037(92)90138-9

Thöni, M., and Miller, C. (1996). Garnet Sm–Nd Data from the Saualpe and the Koralpe (Eastern Alps, Austria): Chronological and P–T Constraints on the Thermal and Tectonic History. *J. Metamorph. Geol.* 14 (4), 453–466. doi:10.1046/j.1525-1314.1996.05995.x

Thöni, M., and Miller, C. (2000). Permo-Triassic Pegmatites in the Eo-Alpine Eclogite-Facies Koralpe Complex, Austria: Age and Magma Source Constraints from Mineral Chemical, Rb-Sr and Sm-Nd Isotope Data. *Schweiz. Mineral. Petrogr. Mittl.* 80 (2), 169–186. doi:10.5169/seals-60959

Thöni, M., and Miller, C. (2004). Ordovician Meta-Pegmatite Garnet (N-W Ötztal Basement, Tyrol, Eastern Alps): Preservation of Magmatic Garnet Chemistry and Sm–Nd Age during Mylonitization. *Chem. Geol.* 209 (1-2), 1–26. doi:10.1016/j.chemgeo.2004.03.006

Thöni, M., and Miller, C. (2009). The "Permian Event" in the Eastern European Alps: Sm–Nd and P–T Data Recorded by Multi-Stage Garnet from the Plankogel Unit. *Chem. Geol.* 260 (1-2), 20–36. doi:10.1016/j.chemgeo.2008.11.017

Thöni, M., and Miller, C. (2010). Andalusite Formation in a Fast Exhuming High-P Wedge: Textural, Microchemical and Sm-Nd and Rb-Sr Age Constraints for a Cretaceous PTT Path at Kienberg, Saualpe Eastern Alps. *Austrian J. Earth Sci.* 103–2.

Thöni, M. (2003). Sm–Nd Isotope Systematics in Garnet from Different Lithologies (Eastern Alps): Age Results, and an Evaluation of Potential Problems for Garnet Sm–Nd Chronometry [Chem. Geol. 185 (2002) 255–281]. *Chem. Geol.* 194 (4), 353–379. doi:10.1016/s0009-2541(02)00419-9

Tofelde, S., Bernhardt, A., Guerit, L., and Romans, B. W. (2021). Times Associated with Source-To-Sink Propagation of Environmental Signals during Landscape Transience. *Front. Earth Sci.* 9–227. doi:10.3389/feart.2021.628315

Tumiati, S., Thöni, M., Nimis, P., Martin, S., and Mair, V. (2003). Mantle–crust Interactions during Variscan Subduction in the Eastern Alps (Nonsberg–Ulten Zone): Geochronology and New Petrological Constraints. *Earth Planet. Sci. Lett.* 210 (3-4), 509–526. doi:10.1016/s0012-821x(03)00161-4

Van Andel, T. H. (1950). *Provenance, Transport and Deposition of Rhine Sediments: A Heavy Mineral Study on River Sands from the Drainage Area of the Rhine*. Wageningen: H. Veenman & Zonen.

Vermeesch, P. (2004). How Many Grains Are Needed for a Provenance Study? *Earth Planet. Sci. Lett.* 224 (3-4), 441–451. doi:10.1016/j.epsl.2004.05.037

von Eynatten, H., and Dunkl, I. (2012). Assessing the Sediment Factory: The Role of Single Grain Analysis. *Earth-Science Rev.* 115 (1-2), 97–120. doi:10.1016/j.earscirev.2012.08.001

Winterberg, S. (2019). Evolution of the Drainage Network in the Greater Alpine Region Assessed with Geomorphic Analyses and Paleo-Geographic Modelling. Doctoral dissertation. Zürich (Switzerland): ETH Zurich.

Wittmann, H., Malusà, M. G., Resentini, A., Garzanti, E., and Niedermann, S. (2016). The Cosmogenic Record of Mountain Erosion Transmitted across a Foreland Basin: Source-To-Sink Analysis of *In Situ* 10 Be, 26 Al and 21 Ne in Sediment of the Po River Catchment. *Earth Planet. Sci. Lett.* 452, 258–271. doi:10.1016/j.epsl.2016.07.017

Yang, Y.-H., Wu, F.-Y., Yang, J.-H., Chew, D. M., Xie, L.-W., Chu, Z.-Y., et al. (2014). Sr and Nd Isotopic Compositions of Apatite Reference Materials Used in U-Th-Pb Geochronology. *Chem. Geol.* 385, 35–55. doi:10.1016/j.chemgeo.2014.07.012

Zhang, J., Sylvester, Z., and Covault, J. (2020). How Do Basin Margins Record Long-Term Tectonic and Climatic Changes? *Geology* 48 (9), 893–897. doi:10.1130/g47498.1

Zweigel, J. (1998). *Eustatic versus Tectonic Control on Foreland Basin Fill: Contributions to Sedimentary Geology*, 20.